

RESEARCH ARTICLE

Snow redistribution onto young sea ice: Observations and implications for climate models

David Clemens-Sewall^{1,*}, Madison M. Smith², Marika M. Holland³, Chris Polashenski^{1,4}, and Don Perovich¹

Vertical heat conduction through young ice is a major source of wintertime sea ice growth in the Arctic. However, field observations indicate that young ice preferentially accumulates wind-blown snow, resulting in greater snow thickness on young ice than would be expected from precipitation alone, and hence greater snow thickness on young ice than climate models represent. As snow has a low thermal conductivity, this additional snow thickness due to redistribution will reduce the actual heat conduction. We present new observations from the Multidisciplinary drifting Observatory for the Study of Arctic Climate Expedition which show that young ice rapidly accumulates a snow thickness of 2.5–8 cm, when wind-blown snow is available from the nearby mature ice. By applying a simple redistribution scheme and heat flux model to simulated conditions from the Community Earth System Model 2.0, we suggest that neglecting this snow redistribution onto young ice could result in the potential overestimation of conductive heat flux—and hence ice growth rates—by 3–8% on average in the Arctic in the winter in the absence of climate feedbacks. The impacts of snow redistribution are highest in the springtime and in coastal regions.

Keywords: Snow, Sea ice, Heat flux, Snow redistribution

1. Introduction

Representing snow on sea ice in climate models is critical for modeling the climate system (Maykut and Untersteiner, 1971; Ledley, 1991; Lecomte et al., 2013; Urrego-Blanco et al., 2016; Webster et al., 2018; Holland et al., 2021). Most climate models represent the sea ice cover within each grid cell as a small number of ice thickness categories, each with their own (laterally homogeneous) snow cover (Hunke et al., 2017; Keen et al., 2021). These ice thickness categories, defined collectively as the 'ice thickness distribution' (Thorndike et al., 1975), represent the sub-grid scale heterogeneity in sea ice thickness and impact the distribution of other properties (e.g., snow thickness). Thermodynamic quantities, including growth/ melt rates and surface fluxes, are computed separately for each ice thickness category within each grid cell. Most sea ice models used in climate models use single, fixed parameters for the snow density and thermal conductivity (e.g., Hunke et al., 2017). Prior work has identified that

Wind-blown snow preferentially accumulates on young ice due to four characteristics of young ice. First, as seawater freezes, a 1–2 mm thick brine skim (**Figure 1a**) develops on the surface of the new ice and is an effective trap for wind-blown snow (Perovich and Richter-Menge, 1994). Second, within hours of the ice freezing under calm conditions, frost flowers—centimeter-scale clusters of dendritic ice crystals (**Figure 1a** and **b**)—grow on the surface of the ice (Perovich and Richter-Menge, 1994). Frost

Email: david.w.clemens-sewall.th@dartmouth.edu

wind-blown snow redistribution between ice thickness categories is an important process to represent in climate models (Lecomte et al., 2015). To our knowledge, Lecomte et al. (2015) provides the only parameterization of subgrid scale snow redistribution on sea ice in a global climate model. The snow redistribution scheme of Lecomte et al. (2015)-which has also been implemented in other climate models (Schröder et al., 2019)-redeposits snow uniformly across thickness categories. However, more than fifty years of field observations indicate that young ice and ridged ice preferentially accumulate wind-blown snow (e.g., Loschilov, 1964; Hanson, 1980; Radionov et al., 1997; Sturm et al., 2002a). Snow is a very effective thermal insulator (Sturm et al., 2002b), and much of the wintertime conductive heat flux in the Arctic is through young ice (Maykut, 1982). Thus, by neglecting wind-blown snow redistribution onto young ice, climate models may be overestimating wintertime conductive heat flux, which may lead to overestimation of Arctic sea ice growth in winter.

¹Thayer School of Engineering, Dartmouth College, Hanover, NH, USA

² Applied Physics Laboratory, University of Washington, Seattle, WA, USA

³National Center for Atmospheric Research, Boulder, CO, USA

⁴Cold Regions Research and Engineering Laboratory, US Army Corps of Engineers, Hanover, NH, USA

^{*}Corresponding author:

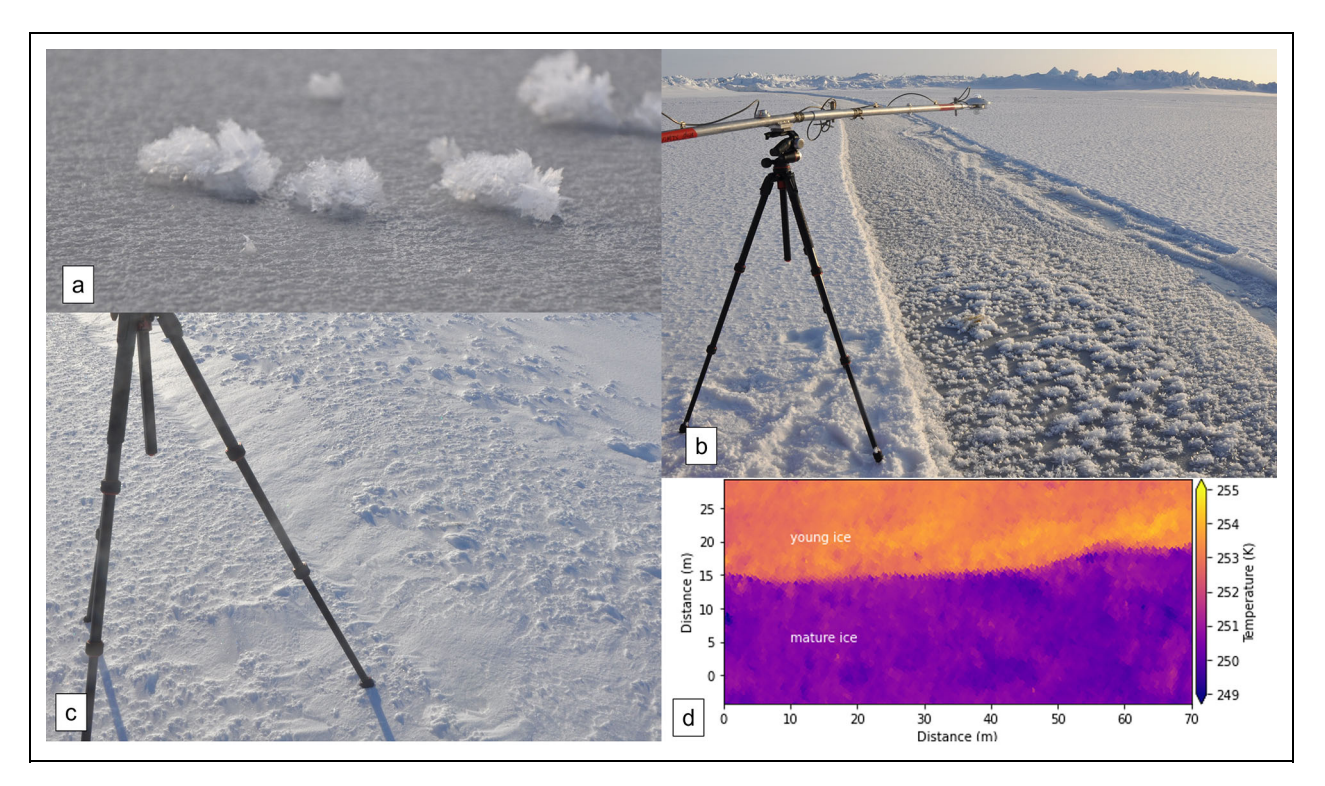


Figure 1. Factors leading to preferential wind-blown snow accumulation on young ice. (a) Brine skim and frost flower formation within hours of ice freezing. (b) Frost flowers with tripod for scale. Note that the surface of the young ice is several centimeters lower than the snow surface surrounding it. (c) The same young ice has accumulated several centimeters of snow after a blowing snow event (tripod in same location as in b). (d) Thermal Infrared image (Thielke et al., 2021) showing that the snow surface above young ice is warmer than the snow surface above mature ice even after snow accumulation. The young ice in (d) is at least 40 cm thick with >8 cm of snow on top of it, whereas the mature ice is approximately 140 cm thick with 25 cm of snow on top of it. The young ice shown in (d) is at a different location than that in (a–c).

flowers create small-scale aerodynamic obstructions which also trap wind-blown snow (Figure 1b and c). Although technically not snow due to their origin as seawater, the frost flowers themselves contribute to the snow layer from a thermodynamic standpoint (Crocker, 1984). Third, once an initial layer of snow has formed, the sintering rate of snow particles should be higher on young ice than mature ice due to higher temperatures. After a snow particle has been deposited, it will begin to sinter, to form ice bonds with adjacent particles. Snow particles that are more sintered are harder for the wind to remobilize. The sintering rate is faster at higher temperatures (Blackford, 2007). And, due to the thinner ice and snow, the snow surface on young ice is warmer than the snow surface on nearby mature ice (e.g., Thielke et al., 2021, also see Figure 1d). Thus, even if the snow deposition rate were the same on mature and young ice, sintering should reduce the remobilization rate on young ice, leading to a net preferential accumulation of wind-blown snow on young ice. Finally, the topographic context in which young ice forms tends to create aerodynamic obstructions that shelter snow on young ice from wind erosion and form snow drifts on young ice. Especially later in the winter, mature ice will have tens of centimeters of snow and ice freeboard, forming a small cliff along the edges of newly frozen leads. Additionally, young ice deforms more easily than mature

ice, and so ice dynamics often build pressure ridges along the edges of leads. The first three characteristics are inherent properties of seawater freezing and thermodynamics and should occur on most or all young ice. The topographic context depends on ice dynamics and other factors, and is not consistent across young ice.

Direct, wintertime observations of snow accumulation on Arctic sea ice are rare, and measurements of snow accumulation on young ice are rarer still. Although limited, the observational record indicates that preferential snow accumulation on young ice occurs at diverse locations and throughout time. At the North Pole Drifting Stations (Loschilov, 1964) and during the Arctic Ice Dynamics Joint Experiment (Hanson, 1980), young ice was observed to accumulate as much snow in 3 months as mature ice did in 7 months or more. However, neither project distinguished how much of this enhanced accumulation rate was due to inherent versus topographic characteristics of young ice. On young ice in Resolute Passage, Canada, Crocker (1984) observed how the growth of frost flowers and trapping of snow generated a uniform snow cover 2-3 cm thick. However, their field site did not include any adjacent mature ice from which wind-blown snow might redeposit. During the Coordinated Eastern Arctic Experiment (Gow et al., 1990; Perovich, 1991) a freezing lead was studied in September and October. Gow et al. (1990) reported snow thickness on the young ice of >5 cm within 5 days of the lead freezing and considerable snow-ice formation, potentially indicating that even more snow had accumulated on the young ice and caused flooding. During the Arctic Leads Experiment (Perovich and Richter-Menge, 1994) the brine skim and frost flowers on newly-frozen lead ice were observed trapping wind-blown snow at four leads in April in the Beaufort Sea. Due to scientific priorities, only the first 3–5 days of ice growth were observed. The Surface Heat Budget of the Arctic (SHEBA) project conducted the most comprehensive wintertime snow observation program (Sturm et al., 2002a; 2002b) prior to the Multidisciplinary drifting Observatory for the Study of Arctic Climate (MOSAiC). However, the physical properties of wintertime leads were not studied. On the Norwegian Young Sea ICE expedition 2 cm of snow were observed on one refrozen lead north of Svalbard (Rösel et al., 2018), but no subsequent observations were made of the snow thickness on this young ice. Collectively, the observational records indicate that young ice preferentially accumulates wind-blown snow and that the surface skim and frost flower trapping mechanisms are ubiquitous. To our knowledge, enhanced sintering has not been observed directly in the field, but warmer snow surface temperatures above young ice are observed routinely (e.g., Figure 1d). Multiple mechanisms contribute to sintering, but all of them lead to an enhanced rate in warmer temperatures (Blackford, 2007).

The sea ice components used in current climate models do not explicitly redistribute snow between thickness categories except during ridging. However, by aggregating all thin ice (e.g., all ice <64 cm as used in CESM2) into the same thickness category with a single, averaged, uniform snow thickness, climate models are implicitly performing snow redistribution on young ice if there is snow-covered ice in the thinnest ice thickness category. Consider a grid cell where 80% of the area is 40-cm thick ice with 10 cm of snow on top of it and the remaining 20% of the area is open water. If the open water were to freeze into 10-cm thick ice, the 'true' grid cell (excluding frost flower growth, wind-blown snow redistribution, and precipitation) would be composed of 20% 10-cm thick ice with 0 cm of snow atop it and 80% 40-cm thick ice with 10 cm of snow. However, the model averages the snow and ice thickness, such that the model grid cell will now be 100% ice with an average thickness of 34 cm with 8 cm of snow on top of it. This implicit snow redistribution has a noticeable effect on thermal conductivity. Assuming purely vertical heat conduction and that the thermal conductivities of snow and ice are $k_s = 0.3 \text{ W m}^{-1} \text{ K}^{-1}$ and $k_i = 2.0 \text{ W m}^{-1} \text{ K}^{-1}$, respectively (the same values used by many climate models; e.g., Hunke et al., 2017), the effective thermal conductivity of the modeled (averaged) grid cell is 8% less than that of the 'true' (not-averaged) grid cell. This implicit snow redistribution is purely a consequence of the resolution of the sub-grid scale ice thickness distribution (the number of thickness categories) and averaging the snow thickness within each thickness category. Note that if there were no ice at the start in the thinnest category, this implicit snow redistribution on young ice would not occur. Most of the models in the latest Coupled Model Intercomparison Project (CMIP6) use five ice thickness categories (Keen et al., 2021)—the same sub-grid scale ice thickness distribution resolution that we use in this work.

Here, we present new observations of snow redistribution onto young Arctic sea ice, a process not currently represented in climate models. We then analyze climate model output to provide evidence that snow redistribution onto young ice impacts climate properties (e.g., heat flux). Finally, we explore the importance of explicitly representing snow redistribution onto young ice for climate modeling.

2. Materials and methods

2.1. Observational data

The MOSAiC project studied a set of drifting ice floes in the Central Arctic from October 4, 2019, through May 16, 2020 (Nicolaus et al., 2022). As part of the MOSAiC expedition, the R/V Polarstern (Alfred-Wegener-Institut Helmholtz-Zentrum für Polar- und Meeresforschung, 2017) drifted along the Transpolar Drift from the northern Laptev Sea into the North Atlantic. Throughout the drift, researchers on board made measurements to characterize the sea ice and snow properties, dynamics, and mass and energy budgets. For a thorough overview of the measurements, see Nicolaus et al. (2022). As part of the MOSAiC expedition, we recorded the dates on which young ice formed and manually measured the snow thickness on this young ice on subsequent dates (**Table 1**). The sharp transitions of the edges of leads and pressure ridges that form from ice dynamics often develop snow drifts, which considerably increase the snow thickness. All of the MOSAiC measurements of snow accumulation on young ice were made far enough away from the lead edges that they were not in snow drifts. Thus, these measurements represent a lower bound of snow thickness on this young ice. Properly incorporating the impact of snow drifts from lead edges in models would require analyzing the sub-grid scale distribution of lead widths and pressure ridges, which is outside the scope of this paper. We estimated snow accumulation rates on mature ice by making repeat measurements of the snow thickness at stakes frozen into the ice (Raphael et al., 2022).

2.2. Model

We used daily snow and ice thicknesses from four ensemble members of the Community Earth System Model 2.0 (CESM2) for the historical period and the 21st century projections (SSP370). Runs performed for the CMIP6 (Eyring et al., 2016) simulate a thin Arctic sea ice relative to observations (DuVivier et al., 2020), and so we utilize simulations in which parameter tuning was applied to improve the Arctic sea ice state (Kay et al., 2022). CESM2 is a state-of-the-art Earth system model, capable of simulating the fully-coupled atmosphere, sea ice, ocean, and land system (Danabasoglu et al., 2020). The sea ice component of CESM2—CICE5 (Hunke et al., 2017)—simulates changes in ice and snow thicknesses and vertical temperature profiles due to conductive, radiative, and turbulent heat fluxes and snow accumulation for each thickness

Table 1. Young ice observed on the MOSAiC expedition^a

Name of Young Ice Location	Date Formed (Year-Month-Day)	Date Measured (Year-Month-Day)	Number of Snow Thickness Measurements	Measurement Spacing (m)
Stakes 1 ^b	2019-11-16 ^c	2019-11-28	10	10
M	2020-03-23	2020-04-18	5	1
SL	2020-03-29	2020-04-15	11	1
ROV Optics ^d	2020-03-29	2020-04-18	11	10
T	2020-04-05	2020-04-15	11	1–2.5

^a These data and a map showing these locations in the MOSAiC Central Observatory are available at Clemens-Sewall (2021). The geographic location where Stakes 1 was measured was approximately 86.1°N, 114°E and the geographic location where M, SL, ROV Optics, and T were measured was approximately 84.5°N, 14°E.

category, assuming that the snow and ice is horizontally uniform within each thickness category and that there are no lateral energy fluxes between categories. The model output includes key parameters of the sea ice state (e.g., snow thickness, ice thickness, ice area fraction) resolved on a daily, per grid-cell, per thickness category basis. The version of CICE used in this work—CICE 5.1.2—is identical to that used in Kay et al. (2022). It includes a Delta-Eddington radiative transfer scheme (Briegleb and Light, 2007), level-ice melt ponds scheme (Hunke et al., 2013),

Table 2. Ice thickness categories in CESM2 runs

Thickness Category	5-Category Lower Bound (m)	15-Category Lower Bound (m)
1	0.00	0.00
2	0.64	0.21
3	1.39	0.44
4	2.47	0.67
5	4.57	0.92
6	na ^a	1.19
7	na	1.50
8	na	1.86
9	na	2.29
10	na	2.84
11	na	3.54
12	na	4.45
13	na	5.66
14	na	7.25
15	na	9.31

^a 'na' refers to 'not applicable'; i.e., the 5-category runs do not have lower category bounds for thickness categories 6–15.

and mushy-layer thermodynamics (Turner and Hunke, 2015). In this work, we examine CESM2 output from runs with two different CICE model setups (**Table 2**): the standard five ice thickness categories (Bitz et al., 2001; Lipscomb, 2001) and a sensitivity run with fifteen ice thickness categories.

2.3. Methods

We estimated the impact that including snow redistribution onto young ice could have on modeled, wintertime conductive heat flux in CESM2 in two steps. First, we applied a simple scheme to redistribute snow between thickness categories in the CESM2 output. Second, we applied a 0-layer thermodynamic model (Semtner, 1976) to estimate the net conductive heat flux throughout the winter in both the standard CESM2 output (without snow redistribution onto young ice) and the output with our snow redistribution onto young ice scheme. These calculations were performed offline on model output, hence they do not feed back onto the climate state.

2.3.1. Snow redistribution scheme

Our field observations indicate that young ice rapidly accumulates a layer of snow (whose thickness we denote as $h_{s,min}$), if wind-blown snow is available. The specific value of $h_{s,min}$ was determined from the *Field observations* in Results. To estimate the available snow at grid cell [j,i] ($v_{s,avail}[j,i]$), we computed the total volume of snow in each grid cell found on ice thickness categories where the snow thickness exceeded $h_{s,min}$, assuming that a fraction (m_{frac}) of this snow was available to be redistributed, using Equation 1:

$$v_{s,avail}[j,i] = m_{frac} \sum_{c=0}^{N_c} I[b_s[c,j,i] > b_{s,min}] b_s[c,j,i] a[c,j,i]$$
 (1)

where N_c is the number of thickness categories, $h_s[c,j,i]$ is the snow thickness on ice thickness category c at grid cell [j,i], $I[b_s[c,j,i] > b_{s,min}]$ is an indicator function (1 if

^b Measurements were made as part of the MOSAiC Mass Balance dataset (Raphael et al., 2022).

^c There is some uncertainty in the formation date of Stakes 1. Due to darkness and logistical constraints, this ice formation was not observed directly and the formation date is based on observations of ice movement nearby. Stakes 1 could have formed up to 2 days after November 16.

^d Measurements were made as part of the MOSAiC Optics dataset (Smith et al., 2021).

 $h_s[c,j,i] > h_{s,min}$; 0 otherwise), and a[c,j,i] is the fractional area of grid cell [j,i] occupied by ice thickness category c. Snow was then added to the thin ice thickness categories (Table 2) such that the snow thickness after redistribution $(b_s[c,j,i]^*)$ was $b_{s,min}$, if that much snow was available, or as much as was available otherwise. The same volume of snow was subtracted evenly (by area fraction) from the thickness categories from which the available snow came. Thus, within each grid cell, snow is neither created nor destroyed, but rather is redistributed from thicker ice categories with thicker snow covers to thinner ice categories with thinner snow covers. Because blowing snow events on Arctic sea ice occur at least a twice a week on average (Loschilov, 1964; Déry and Yau, 1999) and we applied our offline snow redistribution scheme once per week, we are assume that any simulated young ice would have experienced a blowing snow event by the time point at which we applied our offline snow redistribution scheme. An example of the result of our offline snow redistribution scheme is shown in Figure 2.

2.3.2. Zero-layer thermodynamics model heat flux

The zero-layer thermodynamics model (Semtner, 1976) provides estimates of the vertical heat flux through the snow and sea ice assuming that temperatures are in steady-state. By comparing the conductive heat flux with and without snow redistribution onto young ice, we estimated how important this redistribution may be. For each thickness category in each grid cell, we applied the zero-layer model to estimate the conductive heat flux $(F_{cond}[c,j,i])$ for the original snow thicknesses $h_s[c,j,i]$ and the redistributed snow thickness $h_s[c,j,i]^*$, using Equations 2 and 3:

$$F_{cond}[c,j,i] = \frac{k_s(T_o - T_a[j,i])}{h_s[c,j,i] + h_i[c,j,i](k_s/k_i)}$$
(2)

$$F_{cond}[c,j,i]^* = \frac{k_s(T_o - T_a[j,i])}{b_s[c,j,i]^* + b_i[c,j,i](k_s/k_i)}$$
(3)

where $h_i[c,j,i]$ is the per thickness category, per grid cell, ice thickness; T_o is the ice-ocean interface temperature, assumed to be at the freezing point of seawater for the ice growth season considered here; and $T_a[j,i]$ is the per grid cell atmosphere-snow interface temperature in the CESM2 output. The terms k_s and k_i are the thermal conductivities of snow and ice, respectively. We used $k_s=0.3~{\rm W~m^{-1}~K^{-1}}$ and $k_i=2.0~{\rm W~m^{-1}~K^{-1}}$, the same values used in the sea ice component of CESM2 (Hunke et al., 2017). The estimated conductive heat flux $F_{cond}[j,i]$ for each grid cell is then the sum of the thickness category heat fluxes weighted by the fractional area of each ice category a[c,j,i]:

$$F_{cond}[j,i] = \sum_{c=1}^{N_c} F_{cond}[c,j,i] a[c,j,i]$$
 (4)

$$F_{cond}[j,i]^* = \sum_{c=1}^{N_c} F_{cond}[c,j,i]^* a[c,j,i]$$
 (5)

3. Results

3.1. Field observations

The mean snow accumulation observed on young ice at five wintertime leads on the MOSAiC Expedition (**Table 1**) ranged from 2.5 cm to 8 cm, with an average of 6.4 cm and a standard deviation of 2.2 cm (**Figure 3**). During the same time period that the young ice sites M, SL, ROV Optics, and T accumulated snow, the mean snow accumulation on nearby mature ice was 0.5 cm (**Figure 3**). As we observed blowing snow during this time period, we conclude that the preferential snow accumulation on young ice during this time period was due to wind-driven snow redistribution. No contemporaneous measurements of snow accumulation at stakes on mature ice were made

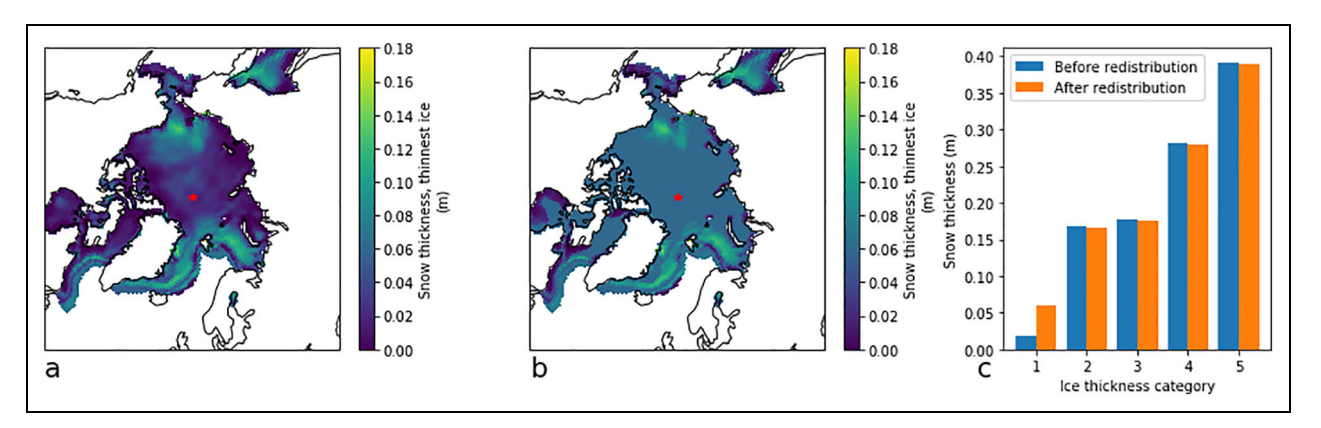


Figure 2. Example of snow thickness (m) on the thinnest ice thickness category in March 2016. Snow thickness (m) on the thinnest ice thickness category in (a) CESM2 output and (b) after applying the offline snow redistribution scheme with $h_{s,min} = 0.06$ m and $m_{frac} = 0.1$. Young ice in much of the Arctic receives some redistributed snow except for parts of the Atlantic and Bering sectors, where the snow thickness before redistribution exceeds $h_{s,min}$. Perthickness category snow thickness in (c) before and after redistribution for a grid cell—red star in (a) and (b) at 157.5°E, 89.7°N—in the Central Arctic. For this grid cell, the thinnest (youngest) ice category occupies only 3.5% of the area, so the addition of 3.7 cm of snow to the thinnest ice category requires the removal of only 0.14 cm of snow from the four thicker ice categories.

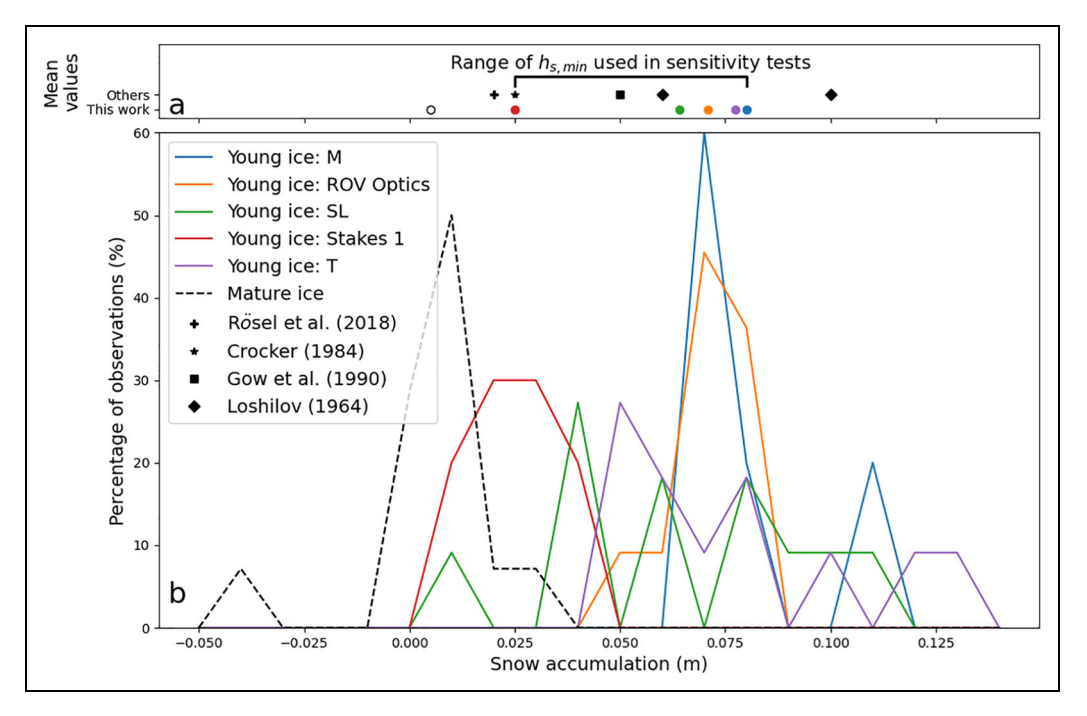


Figure 3. Observations of snow accumulation on wintertime leads. Mean values (a) and distributions (b) of observations of snow accumulation on young ice at five wintertime leads on the MOSAiC Expedition (color-coded by designation: M, ROV Optics, SL, Stakes 1, and T; **Table 1**) compared with snow accumulation on mature ice (dashed line in b) during the same period (except for Stakes 1 where no comparable mature ice observations are available). The mean values (a) of snow accumulation on young ice at each location (solid colored circles) are higher than the mean accumulation observed on mature ice (open circle). These mean values fall in the same range as prior observations (solid black symbols: Loschilov, 1964; Crocker, 1984; Gow et al., 1990; Rösel et al., 2018). Because Loschilov (1964) reported an initial accumulation of 0.1 m followed by a reduction in snow thickness to 0.06 m, both values are shown. The range of $h_{s.min}$ used in the sensitivity tests below is also indicated (a).

during the same time period as the young ice location Stakes 1. These observations of snow accumulation on young ice are consistent with prior observations (**Figure 3**; Loschilov, 1964; Crocker, 1984; Gow et al., 1990; Rösel et al., 2018).

3.2. Impacts of snow redistribution on modelled heat flux

We estimated the conductive heat flux for each climate model grid cell in the Northern Hemisphere with snow redistribution $(F_{cond}[j,i]^*)$ and without $(F_{cond}[j,i])$, weekly from November 1 to May 1, for five winters in four ensemble members, and averaged them to estimate the modeled heat flux for the ice-covered area of the Northern Hemisphere. Four ensemble members and five years were assessed to be sufficient to reduce the impact of internal variability on the basis that at that point the results did not change quantitatively or qualitatively. For example, averaging over three ensemble members and four years yielded a mean potential heat flux overestimation of 6.33%. Averaging over four ensemble members and five years (as presented), the mean potential heat flux overestimation is 6.38%.

The results shown in this section are exclusively from the CESM2 runs with the standard five thickness categories—the same number of thickness categories used in most CMIP6 models (Keen et al., 2021). The ratio of the heat flux without snow redistribution to with redistribution and the difference between them are shown in Figure 4. High heat flux ratios indicate that heat fluxes are currently overestimated by CESM2. These estimates provide an order-of-magnitude assessment of the sensitivity of heat flux in climate models to snow redistribution onto young sea ice. However, because these calculations were performed offline on model output, they do not represent the exact change that one would see in a fully coupled model (due to feedbacks; see Discussion). Computing these exact changes would require implementing snow redistribution in a fully coupled model, which is beyond the scope of the current sensitivity study. We used $b_{s,min} = 0.06$ m, the mean snow thickness from our field observations of young ice. The fraction of the snow volume on Arctic sea ice that is mobile is unknown, but our preliminary analysis from the MOSAiC Expedition suggests that at least 10-20% of the snow volume was redistributed on a weekly basis (data not shown). We thus used $m_{frac} = 0.1$. Neglecting snow redistribution onto young ice leads to a potential overestimation of the conductive heat flux ranging from approximately 1.5% in December to 18% in May with a mean of 6%. The overestimation grows over the course of the winter, as expected, because later in the winter a greater proportion of the conductive heat flux is coming from young ice and more snow is available to redistribute. The magnitude of the difference in

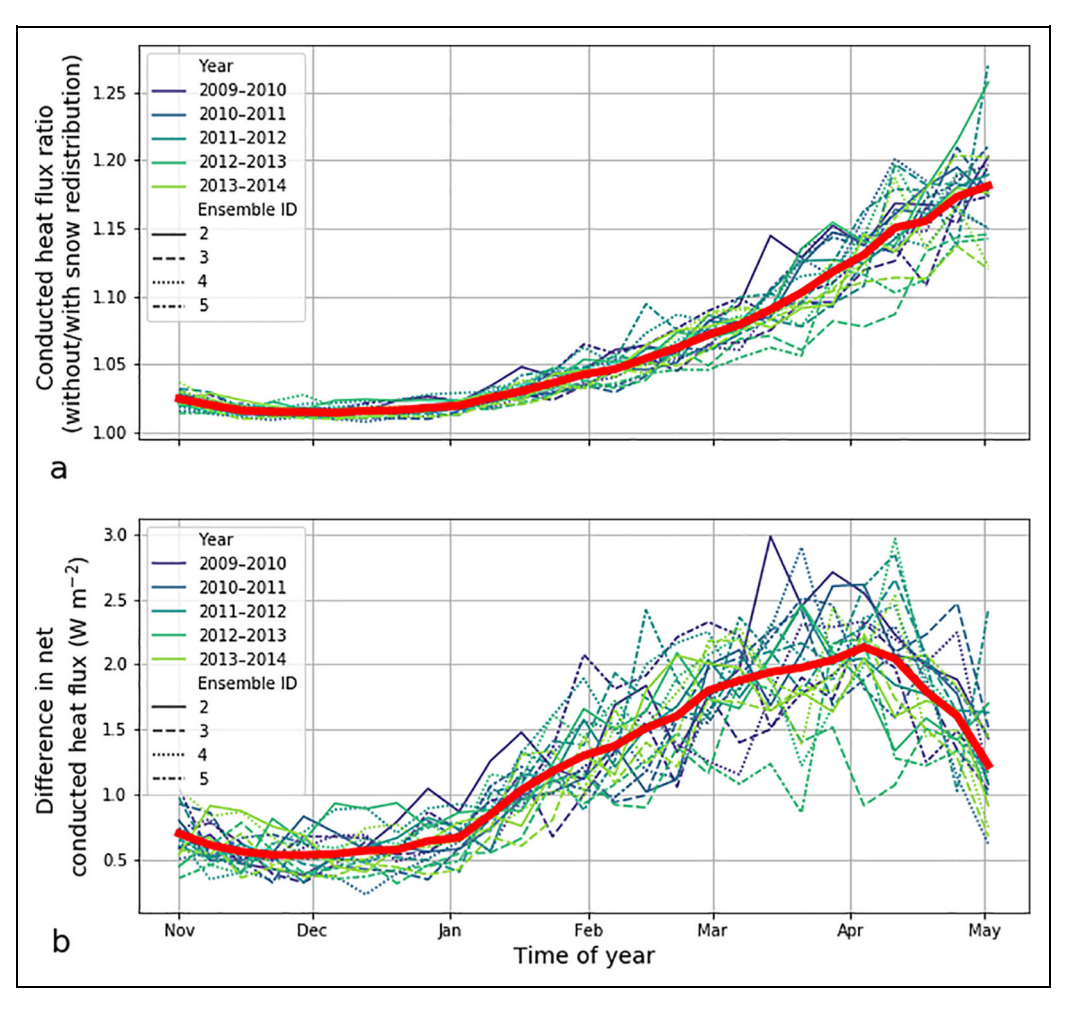


Figure 4. Impacts of snow redistribution on conductive heat flux. The ratio (a) of heat flux without/with snow redistribution and the difference (b) between average heat fluxes over the whole Arctic without and with snow redistribution. Five years and four ensemble members are shown. The red lines show the average of all years and ensemble members. In (a), the heat flux without snow redistribution is always greater than with snow redistribution (all ratios > 1.0).

conductive heat flux peaks in early April, when the atmosphere is still cold and hence the net heat flux is greater than later in the spring.

The spatial patterns of the likely heat flux overestimation (indicated by high heat flux ratios; Figure 5a and b) are driven by a combination of modeled ice deformation, ice thickness distributions, and snow accumulation. Early in the winter season, the only region with notable overestimation is the thick, deforming ice on the north coast of Greenland and the Canadian Archipelago (Figure 5a and i). Overestimation is limited to this region by a combination of where the snow thickness on the young ice without redistribution is less than 6 cm ($b_{s,min}$) and where there is snow on thicker ice available to redistribute (Figure 5c and e). Later in the winter, other coastal regions, where the model simulates more deformation than the Central Arctic, acquire enough ice and snow for heat flux overestimation to occur (not shown). By springtime, overestimation occurs throughout the Arctic Basin and only some regions of the marginal seas are excluded (Figure 5b). Snow thickness on young ice without redistribution is mostly less than 6 cm (Figure 5d; some

exceptions in the Greenland, Barents, and Chukchi seas), and there is snow available to redistribute from thicker ice almost everywhere (**Figure 5f**). In both December and April, the fraction of heat flux that comes from the thinnest ice category (**Figure 5g** and **h**) modulates the intensity of the overestimation. In April, the region with the greatest overestimation is the Beaufort Sea (18% overestimation) followed by the Kara, East Siberian, and Laptev seas (all of which have approximately 16% overestimation). These results highlight that snow redistribution onto young sea ice is most important near the coasts but the exact regional distribution is also impacted by the accuracy with which the model simulates sea ice deformation (see Discussion).

We assessed the sensitivity of these results to the parameters of minimum snow thickness on young ice $(h_{s,min})$ and fraction of the snow volume that is mobile (m_{frac}) by testing a range of values for these parameters (**Figures 6** and **7**). For the $h_{s,min}$ sensitivity test, we set the mobile fraction of snow at 0.1 and tested $h_{s,min}$ from 0.025 to 0.08 m—the range of minimum snow accumulation that we observed in our field observations. Then, for each value

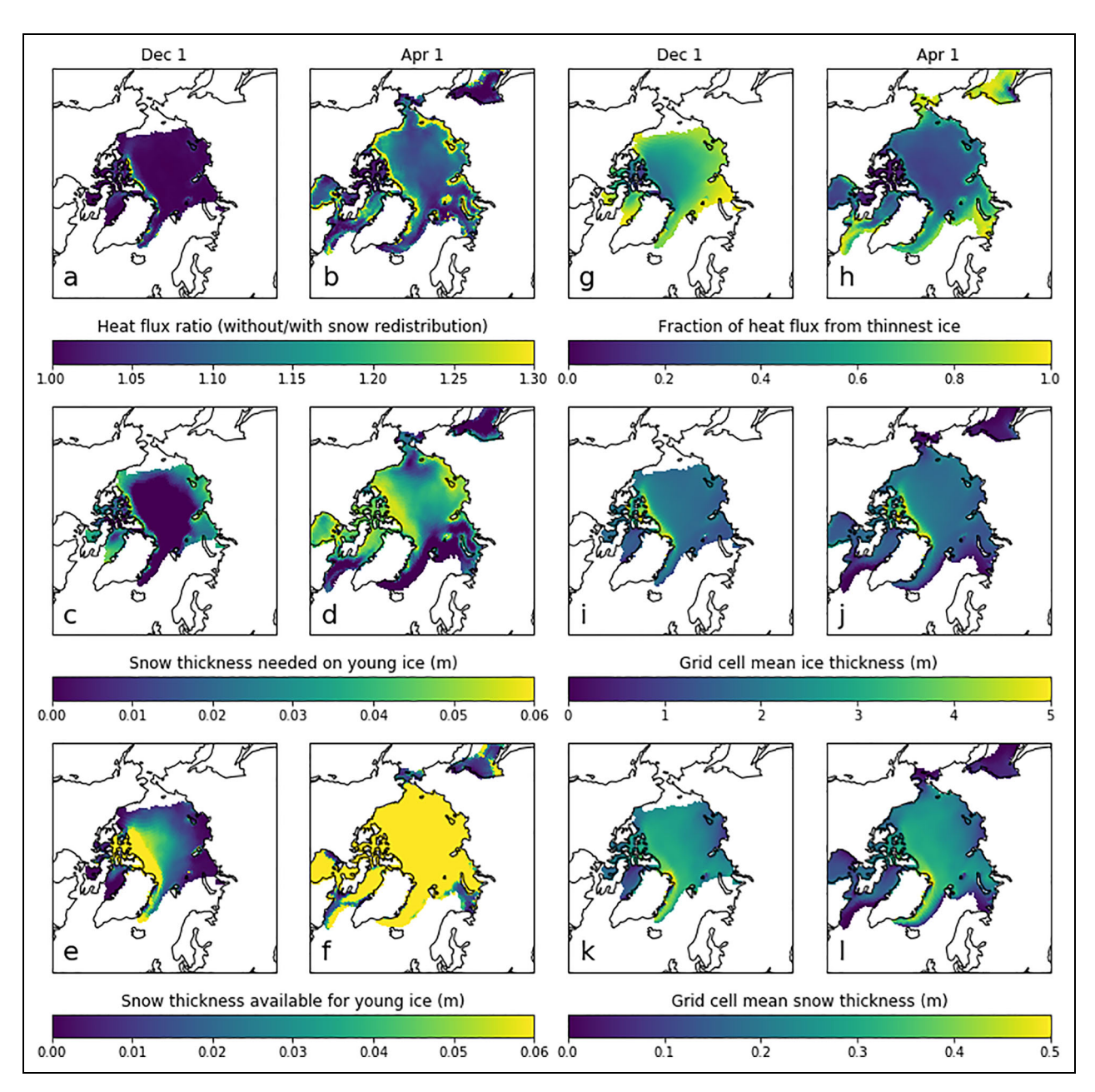


Figure 5. Spatial patterns of heat flux overestimation and factors that contribute to it. Maps of the ratio of heat flux with and without snow redistribution (a, b); the amount of snow needed to raise the snow thickness on young ice to $h_{s,min}$ (c, d); the amount of snow available to redistribute (e, f); shown in terms of how much it would raise the snow thickness on young ice if all of the available snow were redistributed (solid yellow regions indicate that greater than $h_{s,min}$ is available), the fraction of the total heat flux emanating from the thinnest ice category (g, h); the ice thickness (i, j); and the snow thickness (k, l) for the dates December 1 (a, c, e, g, i, k), and April 1 (b, d, f, h, j, l). Data have been averaged across four ensemble members and the years 2009–2014 to reduce the impact of internal variability.

of $h_{s,min}$, we applied our snow redistribution scheme and the zero-layer thermodynamics model to estimate conductive heat flux for all four ensemble members and five years as described above. The m_{frac} sensitivity tests were conducted in the same manner except that we set $h_{s,min}$ to 0.06 m and tested m_{frac} from 0.01 to 0.3. Because the mobile fraction of snow on Arctic sea ice is not known, we relied upon a preliminary analysis of Terrestrial Laser Scanning data from the MOSAiC Expedition which suggested a value between 0.1 and 0.2. Given the uncertainty,

we tested lowering the mobile fraction an order of magnitude, to 0.01, and still found impacts on the estimated heat flux. Varying the parameter values impacts the magnitudes, but not the patterns of the overestimation in the heat flux ratio. For the range of parameter values tested, the wintertime mean heat flux ratio (averaged across the Arctic) ranged from 1.03 to 1.08. Snow redistribution onto young ice had the greatest impact in April, when the Arctic-averaged heat flux overestimation could be as high as 15%.

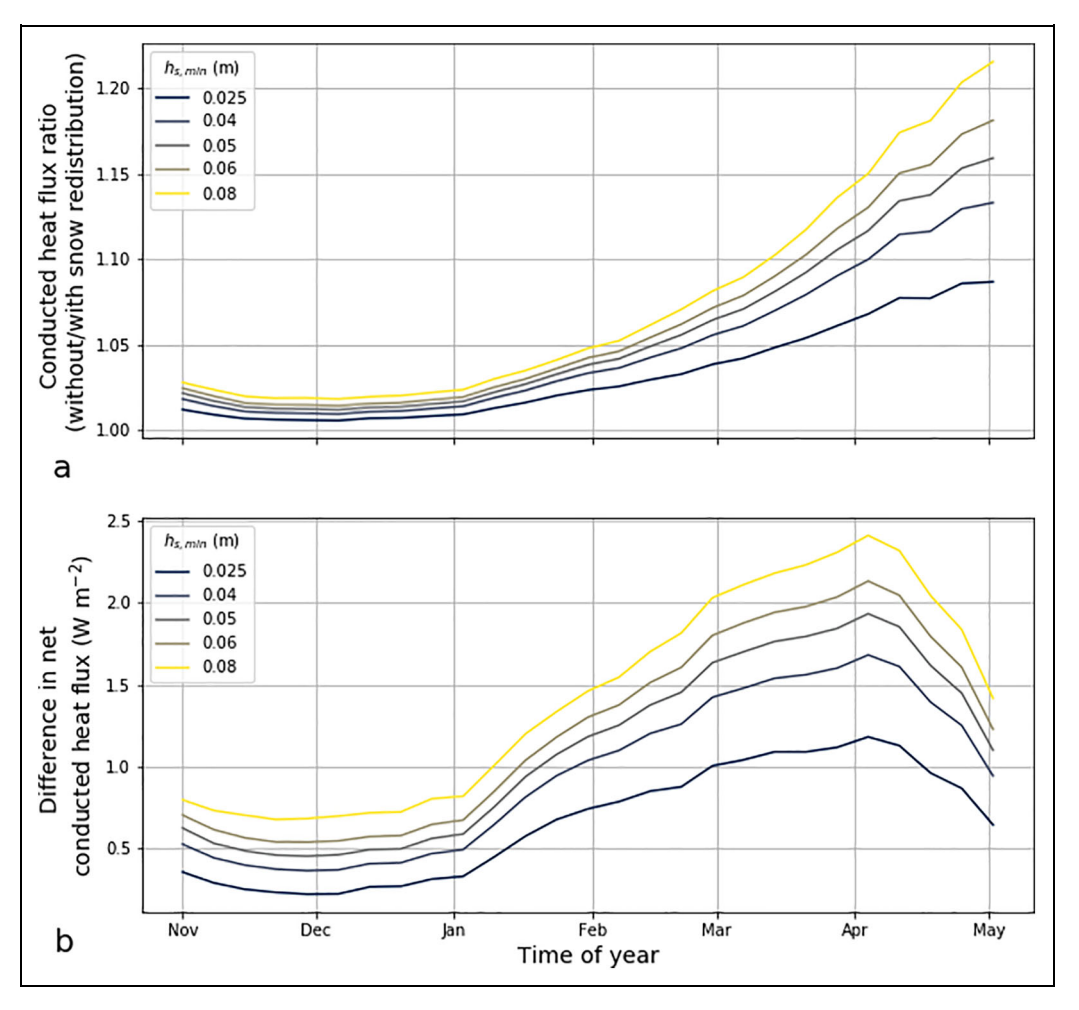


Figure 6. Sensitivity of heat flux overestimation to $h_{s,min}$. The ratio (a) of heat flux without/with snow redistribution and the difference (b) between average heat fluxes without and with snow redistribution for different values of minimum snow thickness on young ice ($h_{s,min}$). The five years and four ensemble members shown in **Figure 4** have been averaged together.

4. Discussion

4.1. Importance of snow redistribution onto young ice

The results presented here suggest that wind-blown snow redistribution onto young sea ice may be an important process to represent explicitly in coupled climate models. In the present-day climate, neglecting preferential snow accumulation on young ice in CESM2 could lead to overestimating the conductive heat flux, averaged across the Arctic, by 1.5–18% with the largest impacts in the late winter and springtime. The field observations presented herein combined with the results from Loschilov (1964), Crocker (1984), Gow et al. (1990), and Rösel et al. (2018) all support that $h_{s,min}$ falls in the range of 0.02 to 0.1 m. The lower bound of this range is likely due to the effects of brine skim and frost flowers on the surface of young ice (Perovich and Richter-Menge, 1994). Because the mobile fraction of snow on sea ice is harder to constrain, we explored the sensitivity of snow redistribution onto young ice to a wide range of m_{frac} from 0.01 to 0.3 (1% to 30%). Studies have suggested that blowing snow could lead to the loss of 30% to 50% of the snow on sea ice from blowing-snow sublimation (Déry and Tremblay, 2004) or from blowing snow into leads (Leonard and Maksym, 2011). Although these values are not directly comparable, they are clearly consistent with greater than 1% of the snow redistributing.

Two processes limit the availability of snow that can be redistributed, and both tend to limit the overestimation effect early in the season. First, the thicker ice needs to have accumulated enough snow to exceed significantly the minimum snow thickness in our redistribution scheme. Second, the thicker ice categories need to occupy sufficient area of the grid cell for there to be enough volume of snow to redistribute. If the thinnest ice category comprises most of the ice area, then there will not be enough snow volume for redistribution to change significantly the snow thickness on the thinnest ice. The lack of available snow (Figure 5e dark areas) reduces the importance of snow redistribution across most areas of the Arctic where thin ice lacks snow early in the winter (Figure 5c light areas). The proportion of heat flux from the thinnest ice category depends on the ice thickness distribution which, in turn, is impacted by ice age and dynamics. Thus the areas of greatest overestimation are in coastal regions where ice dynamics create thick ice and thin ice. The

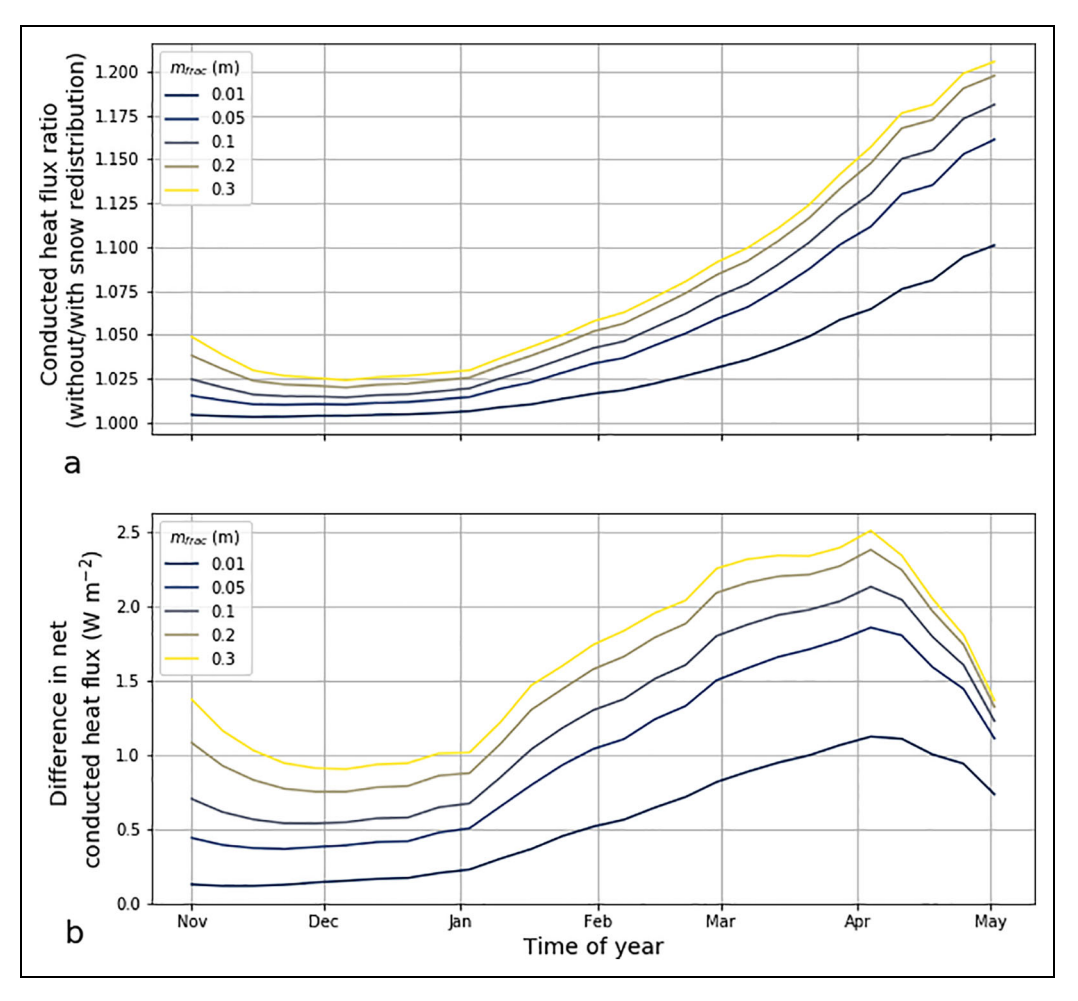


Figure 7. Sensitivity of heat flux overestimation to m_{frac} . The ratio (a) of heat flux without/with snow redistribution and the difference (b) in average heat flux without and with snow redistribution for different values of the mobile fraction of the snow volume (m_{frac}). The five years and four ensemble members shown in **Figure 4** have been averaged together.

spatial patterns of potential heat flux overestimation emphasize that the magnitude of ice deformation impacts the importance of snow redistribution onto young ice; however, the exact values of the potential heat flux overestimation (e.g., 18% overestimation in the Beaufort Sea in April) should not be taken literally because the horizontal resolution of the grid used in CESM2 (1°) is relatively coarse. Observations and higher-resolution models (e.g., Spreen et al., 2017) suggest that coarse models underestimate the amount of ice deformation, especially near the coast. Better simulation of sea ice deformation may shift which coastal regions experience the greatest heat flux overestimation but will not change the overall pattern of this snow redistribution process being more important near the coasts.

4.2. Comparison with other uncertain snow properties

Snow redistribution on Arctic sea ice is not the only process that is currently underrepresented in climate models which may impact heat flux. The standard version of CICE represents all snow on sea ice as having a single uniform density and thermal conductivity, although field

observations (e.g., Sturm et al., 2002a; 2002b) have shown considerable variation in both material properties. Here we have applied the same offline zero-layer thermodynamics model developed above (Equation 2), but instead of redistributing the snow thickness between categories, we adjusted the material property (e.g., thermal conductivity) in Equation 6:

$$F_{cond}[c,j,i]^{k} = \frac{k_{s}^{*}(T_{o} - T_{a}[j,i])}{h_{s}[c,j,i] + h_{i}[c,j,i](k_{s}^{*}/k_{i})}$$
(6)

where $F_{cond}[c,j,i]^k$ is the per-grid cell, per-ice thickness category heat flux if the snow thermal conductivity is k_s^* . Calonne et al. (2019) found that at snow densities of 300 kg m⁻³ the thermal conductivity of snow samples varied by 0.08 W m⁻¹K⁻¹. Applying this range in our off-line scheme suggests that this uncertainty in the thermal conductivity of snow translates to an Arctic-averaged potential heat flux uncertainty ranging from 4% underestimation to 5% overestimation (purple lines in **Figure 8**). Snow density on Arctic sea ice is also uncertain, and CICE currently uses a fixed value of 330 kg m⁻³. Sturm et al. (2002a) measured the average bulk density at 29 sites dispersed around the SHEBA Expedition and found a range

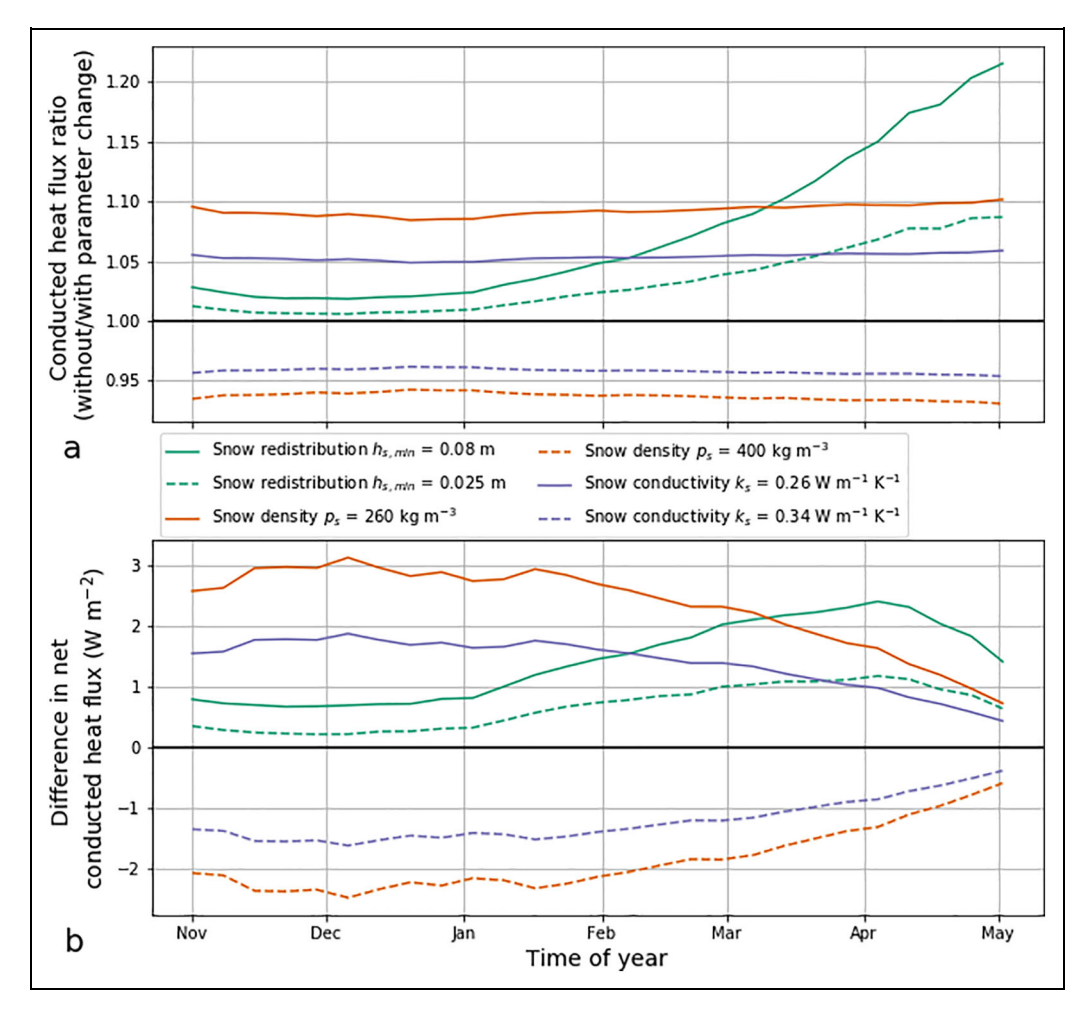


Figure 8. Comparison of snow redistribution onto young ice with uncertainties in density and thermal conductivity. The ratio (a) of heat flux without/with changes in either the snow redistribution, snow density, or snow thermal conductivity and the difference (b) between average heat fluxes without and with these parameter changes. The years 2009–2014 and four ensemble members have been averaged together to reduce the impact of internal variability. The teal solid lines are identical to yellow lines in **Figure 6** and the teal dashed lines are identical to the black lines in **Figure 6**.

in bulk densities from 260 to 400 kg m $^{-3}$. When we conserved snow mass and used this range of densities to change the snow thickness in our offline scheme, our results suggest that this uncertainty in the density of snow translates to an Arctic-averaged potential heat flux uncertainty ranging from 6% underestimation to 9% overestimation (orange lines in **Figure 8**).

Figure 8 shows a comparison between the uncertainties in snow redistribution onto young Arctic sea ice and the aforementioned uncertainties in density and thermal conductivity. This comparison reveals three findings. First, the magnitude of the impacts of snow redistribution onto young sea ice are similar in order-of-magnitude to the impacts of the uncertainty in snow density and thermal conductivity. Second, the impacts of snow redistribution onto young sea ice exhibit a springtime peak, unlike density or thermal conductivity. Third, our uncertainty in snow density and thermal conductivity suggest that climate models could be overestimating or underestimating conductive heat flux due to these properties. However, because snow redistribution onto young ice is not

represented explicitly in climate models, our results suggest that climate models are overestimating conductive heat flux due to the omission of this specific process.

4.3. Sensitivity to model setup

There are two reasons why the modeled snow thickness on thin ice may exceed $h_{s,min}$. First, the precipitation rate may simply be high enough that new ice rapidly accumulates a thick layer of snow in the model. This effect should be most prominent in the fall when snow precipitation rates are highest. Second, the implicit snow redistribution induced by averaging snow thickness within each ice thickness category may be sufficiently effective at redistributing snow onto young ice to reduce the impacts of not explicitly representing snow redistribution in the model. To explore the importance of this effect, we examined the overestimation of heat flux due to neglecting snow redistribution onto young ice in a CESM2 run with fifteen ice thickness categories instead of the standard five categories (Figure 9). In the fifteen category output, we find that the potential heat flux overestimation is greater and begins

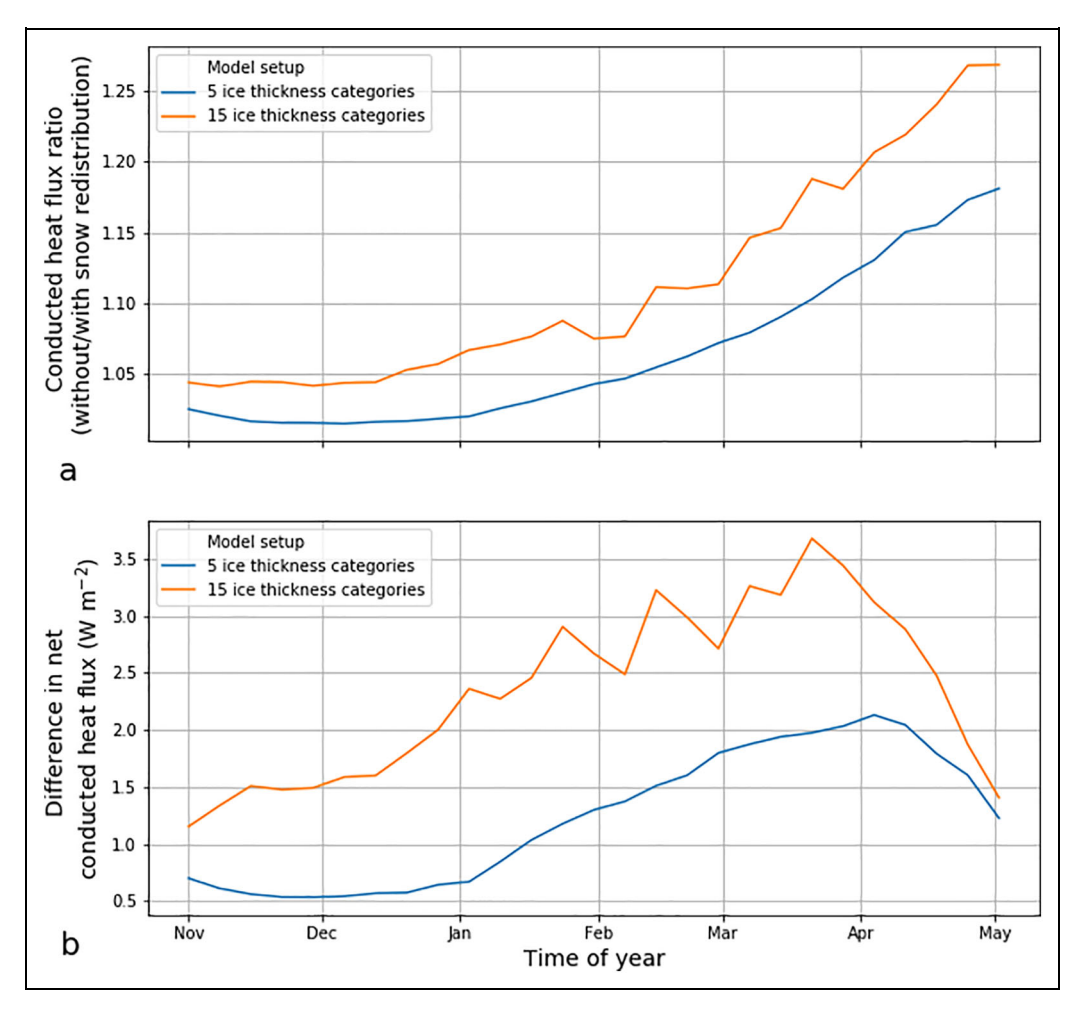


Figure 9. Sensitivity of heat flux to the number of ice thickness categories. The ratio (a) of heat flux without/with snow redistribution and the difference (b) between average heat fluxes without and with snow redistribution in the standard model setup with five ice thickness categories (blue line) and a model run with fifteen thickness categories (orange line). The years 2009–2014 have been averaged together to reduce the impact of internal variability. For the five category model output, four ensemble members have been averaged together (same as the red lines in **Figure 4**).

earlier in the winter. These differences are due to a combination of factors: increasing the model's thickness resolution reduces the effectiveness of implicit snow redistribution within thickness categories and the sea ice cover in the fifteen category run is thicker than in the standard, five category model. In the latter case, all of the young ice is in a single category where its snow thickness is averaged across the entire category. Thus, when new ice is added, the model implicitly redistributes snow and ice volume from slightly thicker ice (up to 64 cm) onto this thinnest ice. This implicit snow redistribution becomes less effective when we have more ice thickness categories, because the snow thickness is being averaged across a smaller range of ice thicknesses. Thus, when we compare results of the implicit snow redistribution (due to averaging in the model) with the explicit snow redistribution scheme described above, we find that increasing the number of thickness categories increases the average potential heat flux overestimation from 6% to 11%. The exact numerical results are not critical, but the relative change (a little under a doubling of the impact) highlights that snow redistribution onto young ice is sensitive to the model setup.

4.4. Sensitivity to modeled climate state

For computational reasons, coupled climate models often aggregate multiple sub-grid scale processes into single explicit representations. For example, CESM2 represents all heat flux in the snow on sea ice as vertical, one-dimensional conduction with a single 'aggregated' thermal conductivity, rather than explicitly modeling the heat conduction through the ice grain lattice and interstitial air in the snow, heat flux due to vapor transport in the snow cover (Calonne et al., 2011), and enhanced heat flux due to the floe-scale spatial distribution of snow (Sturm et al., 2002a; 2002b). The 'aggregated' thermal conductivity of snow on sea ice used in CICE (Hunke et al., 2017) is approximately double the value measured by field observations (Sturm et al., 2002b) to account for these nonconductive and threedimensional processes. This approach is sensible for processes that are unlikely to change in response to either a changing climate state or changing model setup.

To investigate whether snow redistribution onto young ice could be aggregated with other processes (e.g., by reducing the thermal conductivity of snow on thin ice categories) or should be represented explicitly, we examined the potential overestimation of heat flux from the 1970s through the 21st century projections (SSP370; Figure 10). The purpose of these comparisons is to investigate whether the process of snow redistribution onto young ice is sensitive to the climate state, not to predict how this process will behave at any particular point in time. In warmer climate states, the magnitude of the overestimation of heat flux generally decreases due to the forced climate warming response. As the climate warms, the area fraction of thicker ice categories and the snow thickness decline on average. In effect, a warming climate causes the thinner snow and ice conditions that historically prevailed early in the winter season to be prevalent later and later into the winter. Thus, the simulated response is consistent with the spatial and temporal patterns we have observed in our analysis of present-day model output and suggests that snow redistribution onto young ice is sensitive to changes in the climate state.

4.5. Interaction with feedbacks

The importance of snow redistribution changes with different model setups (e.g., a different number of ice thickness categories; **Figure 9**), and the potential impacts of snow redistribution change in future climate states (**Figure 10**). Because the potential effects of snow redistribution change with changing climate and model setups, we suggest that future researchers test the sensitivity of a coupled climate model to an explicit parameterization of snow redistribution onto young ice. Although there are multiple valid ways one might implement an explicit parameterization of snow redistribution onto young ice, testing parameterizations and detailed analysis of the impacts and feedbacks of this model change are beyond the scope of this study.

However, we have adapted this offline approach to explore the effects of the sea ice thickness feedback (Bitz and Roe, 2004; Petty et al., 2018; Ricker et al., 2021), a negative feedback by which thinner ice conducts more heat flux from the ocean to the atmosphere in the winter. The offline analysis presented thus far does not account for how the reduction in heat flux will produce thinner

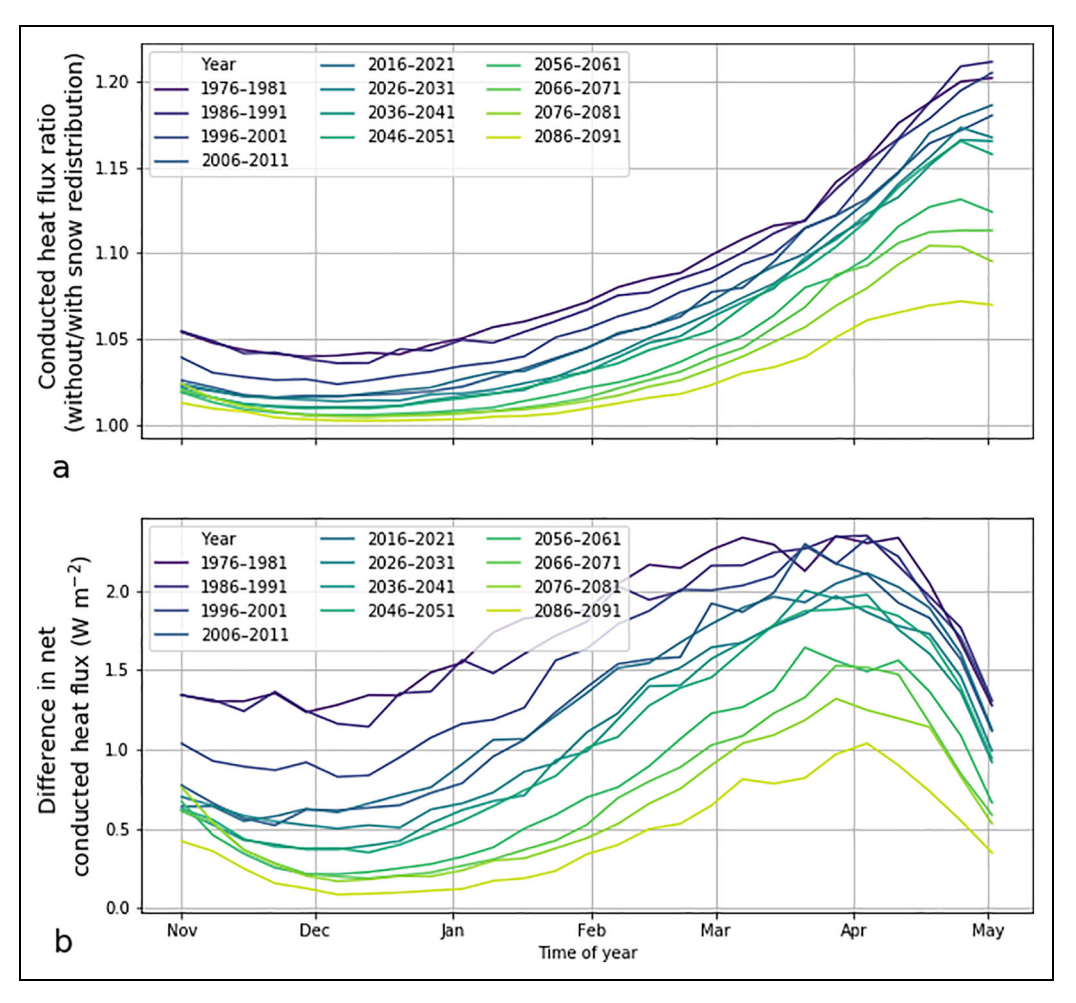


Figure 10. Sensitivity of snow redistribution impacts to different climate states. The ratio (a) of heat flux without/with snow redistribution and the difference (b) between average heat fluxes without and with snow redistribution from the 1970s through the 21st century projections from a four member ensemble of CESM2 under the RCP 8.5 emissions scenario (for the future projections). Five consecutive years from each decade and all four ensemble members have been averaged together to account for internal variability.

ice, which, in turn, will conduct slightly more heat (see Equation 3). This effect is limited by how much the snow redistribution reduces the heat flux and hence ice growth. **Figure 11** shows an estimate of the maximum amount by which this feedback could reduce the potential overestimation of heat flux (blue line) whereby the ice thickness is reduced by the same percentage as the simulated reduction in heat flux from snow redistribution (Figure 4). In this scenario, the Arctic-averaged potential heat flux overestimation is just 2%; however, the ice is 15% thinner in the springtime which will have other significant impacts on the Arctic system. Because the ice would then grow slightly thicker under this scenario, the actual heat flux overestimation will fall somewhere between the maximum ice feedback scenario (blue line in **Figure 11**) and the no ice feedback scenario (red line in Figure 11). This process is strictly self-limiting and can impact the magnitude of the heat flux overestimation but not the sign, as there is no mechanism by which this particular feedback could lead snow redistribution onto young ice to increase the net conducted heat flux.

If snow redistribution onto young ice were represented explicitly in climate models, its impact on the sea ice state would be modulated by a number of additional positive and negative feedback processes with net impacts that are harder to predict (Figure 12). The two immediate impacts of redistributing snow onto young ice are straightforward to predict. Including this snow redistribution will reduce wintertime conductive heat flux (decreasing young ice growth) and increase albedo on young ice in the spring and early summer (decreasing young ice melt). However, the net downstream impacts of the change cannot be predicted without a coupled ice-atmosphere-ocean model, as highlighted by Figure 12. Reducing heat flux directly decreases the amount of congelation ice growth. Thinner ice also melts completely to reveal open water, increasing ice loss through the ice-albedo feedback. However, reduced heat flux will result in a colder atmosphere, which, if all else were equal, would increase ice growth rates and delay melt onset-a negative feedback. The increased albedo on young ice will reduce spring and early summer radiation absorption, potentially delaying the

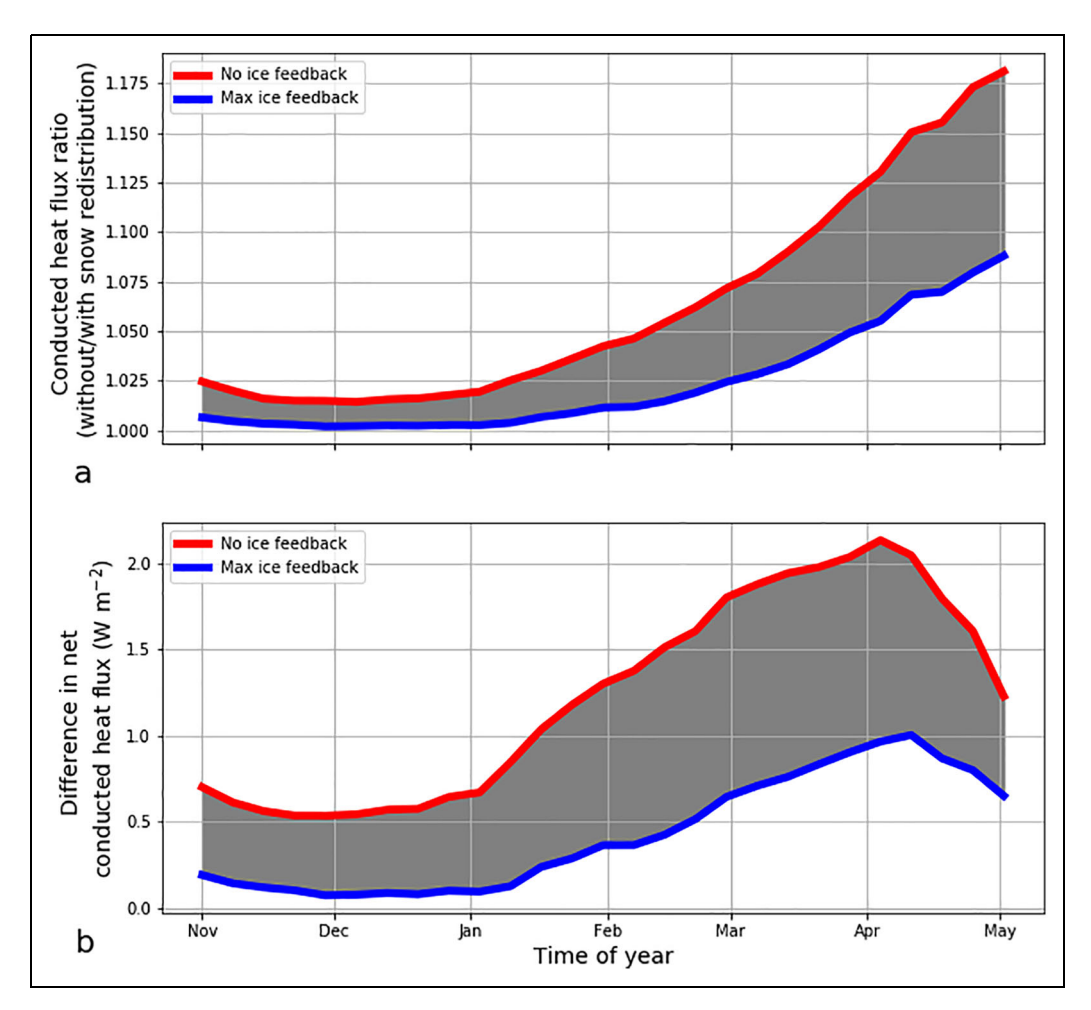


Figure 11. Potential impacts of ice-thickness feedback. Scenarios for how the ice thickness feedback may impact the ratio (a) of heat flux without/with snow redistribution and the difference (b) between average heat flux without and with snow redistribution. The 'no ice feedback' scenario (red lines) is identical to the red lines in **Figure 4**. The 'max ice feedback' scenario (blue lines) is how the heat flux would change if the ice thickness were reduced by simulated reduction in heat flux. As described in the text, the net impact will fall between these scenarios (grey shaded area).

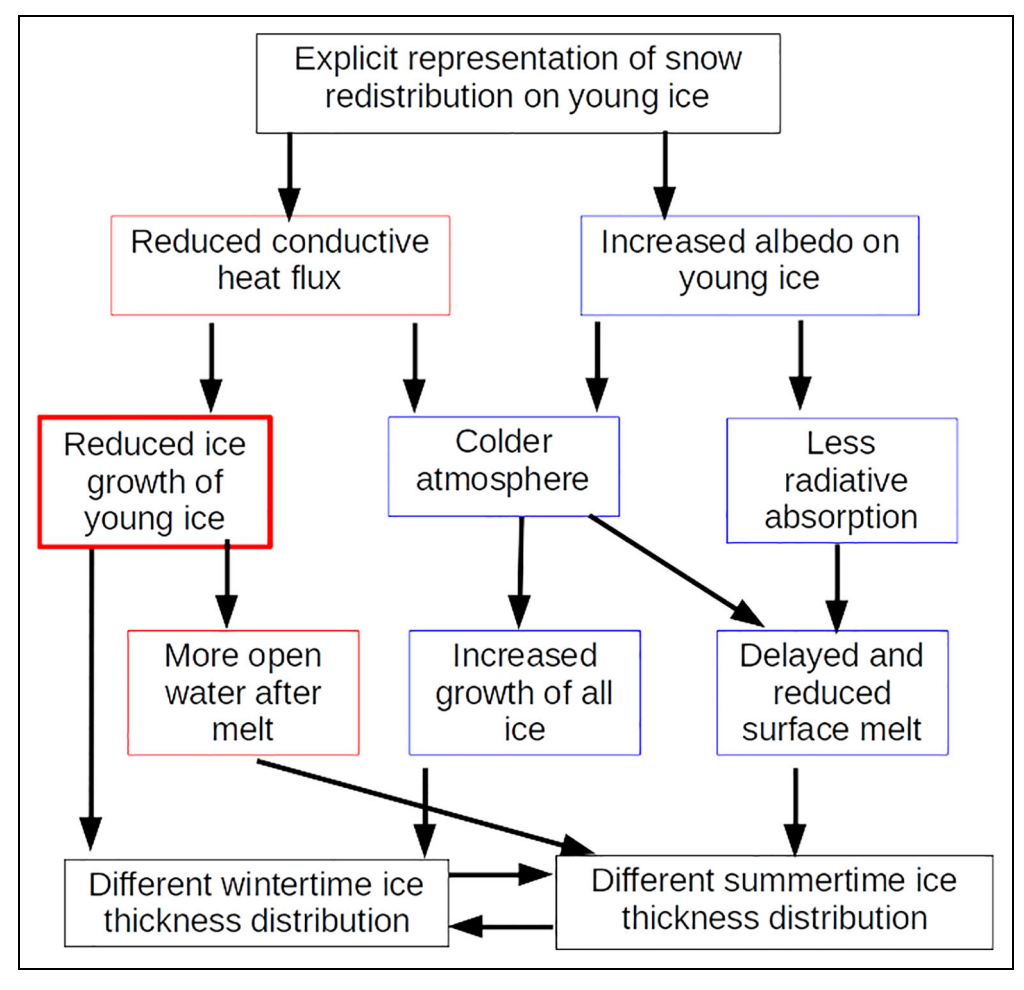


Figure 12. Potential coupled climate feedbacks. Feedbacks that would impact sea ice state if snow redistribution on young ice were represented explicitly in a coupled climate model. Reduced growth of young ice is highlighted because it likely has the largest single impact on sea ice state.

start of surface melt and reducing ice melt—another negative feedback. These feedbacks will interact with other feedbacks in the Arctic sea ice system. Modeling the interactions of processes and feedbacks such as these is critical to understanding how Arctic sea ice may respond to a changing climate.

5. Conclusion

We have presented new field observations and reviewed prior observations to show that young sea ice preferentially accumulates 2.5-8 cm of wind-blown snow due to a combination of brine skim, frost flowers, enhanced sintering rates due to warmer snow surfaces, and topographic effects from aerodynamic obstacles on lead edges. Applying an offline (excluding coupled climate feedbacks) snow redistribution scheme to CESM2 model outputs allowed us to determine that neglecting this snow redistribution process potentially causes the model to overestimate wintertime conductive heat flux by 1.5% to 18% depending on time of year, averaged across the Arctic Basin. The magnitude of this potential heat flux overestimation is similar to the magnitude of heat flux uncertainty due to uncertainties in snow density and thermal conductivity on Arctic sea ice. Snow redistribution onto young ice is most important in coastal areas where ice deformation creates large areas of young ice at times when there is snow available to redistribute. Furthermore, the magnitude of this potential overestimation changes with different climate states and different model setups—indicating that it cannot be addressed by tuning the mean state of the model. Future work should consider parameterizing snow redistribution onto young ice within coupled climate models.

Data accessibility statement

The data analyzed in this work are available at the Arctic Data Center or PANGAEA and cited throughout. The version of CICE (Hunke et al., 2017) used in this work is available here: https://github.com/ESCOMP/CESM_CICE5/releases/tag/cice5_cesm2_1_1_20190321.

Acknowledgments

Data used in this article were produced as part of the international MOSAiC project with the tag MOSAiC 220192020 and the Project_ID: AWI_PS122_00. We thank all people involved in the expedition of the research vessel *Polarstern* during MOSAiC in 2019–2020 as listed in Nixdorf et al. (2021). For the Community Earth System

Model simulations, we acknowledge computing and data storage resources, including the Cheyenne supercomputer (DOI: http://dx.doi.org/10.5065/D6RX99HX), which were provided by the Computational and Information Systems Laboratory at NCAR. NCAR is sponsored by the National Science Foundation. We thank Philip Anhaus, Eric Brossier, Jennifer Hutchings, Thomas Olufson, Ian Raphael, Saga Svavarsdottir, and Julia Schmale for their capable assistance in the field and Linda Thielke for providing the Thermal IR image in **Figure 1d**. We also thank Jody Deming, Marcel Nicolaus, Frank Kauker, and an anonymous reviewer for their helpful suggestions.

Funding

DCS, DP, and CP were supported by NSF OPP-1724540, NSF OPP-2034919, and ONR N00014-19-1-2603. MMS was supported by NSF OPP-1724467 and OPP-1724748. MMH was supported by NSF OPP-1724748.

Competing interests

None.

Author contributions

- Contributed to conception and design: DCS (study as a whole), MMH (model study), DP & CP (field observations).
- Contributed to acquisition of data (including CESM2 simulations): DCS, MMS.
- Contributed to analysis and interpretation of data: DCS, MMH, DP, CP, MMS.
- Drafted and/or revised the article: DCS, MMH, DP, CP, MMS.
- Approved the submitted version for publication: DCS, MMH, DP, CP, MMS.

References

- Alfred-Wegener-Institut Helmholtz-Zentrum für Polar- und Meeresforschung. 2017. Polar research and supply vessel POLARSTERN operated by the Alfred-Wegener-Institute. *Journal of Large-Scale Research Facilities* 3: A119. DOI: http://dx.doi.org/10.17815/jlsrf-3-163; http://jlsrf.org/index.php/lsf/article/view/163.
- **Bitz, CM**, **Holland**, **MM**, **Weaver**, **AJ**, **Eby**, **M**. 2001. Simulating the ice-thickness distribution in a coupled climate model. *Journal of Geophysical Research: Oceans* **106**(C2): 2441–2463. DOI: http://dx.doi.org/10.1029/1999JC000113; https://onlinelibrary.wiley.com/doi/abs/10.1029/1999JC000113.
- **Bitz, CM, Roe, GH**. 2004. A mechanism for the high rate of sea ice thinning in the Arctic Ocean. *Journal of Climate* **17**(18): 3623–3632. DOI: http://dx.doi.org/10.1175/1520-0442(2004)017<3623:AMFTHR>2.0. CO;2; https://journals.ametsoc.org/view/journals/clim/17/18/1520-0442_2004_017_3623_amfthr2. 0.co_2.xml.
- **Blackford, JR**. 2007. Sintering and microstructure of ice: A review. *Journal of Physics D: Applied Physics*

- **40**(21): R355–R385. DOI: http://dx.doi.org/10. 1088/0022-3727/40/21/R02.
- Briegleb, B, Light, B. 2007. A Delta-Eddington mutiple scattering parameterization for solar radiation in the sea ice component of the community climate system model. University Corporation for Atmospheric Research. DOI: http://dx.doi.org/10.5065/D6B2 7S71. Available at http://opensky.ucar.edu/islandora/object/technotes:484.
- Calonne, N, Flin, F, Morin, S, Lesaffre, B, Roscoat, SRd, Geindreau, C. 2011. Numerical and experimental investigations of the effective thermal conductivity of snow. *Geophysical Research Letters* **38**(23). DOI: http://dx.doi.org/10.1029/2011GL049234; https://agupubs.onlinelibrary.wiley.com/doi/abs/10.1029/2011GL049234.
- Calonne, N, Milliancourt, L, Burr, A, Philip, A, Martin, CL, Flin, F, Geindreau, C. 2019. Thermal conductivity of snow, firn, and porous ice from 3-D image-based computations. *Geophysical Research Letters* **46**(22): 13079–13089. DOI: http://dx.doi.org/10. 1029/2019GL085228; https://agupubs.onlinelibrary.wiley.com/doi/abs/10.1029/2019GL085228.
- Clemens-Sewall, D. 2021. Snow thickness measurements on young ice in the Central Arctic during the 2019–2020 Multidisciplinary Drifting Observatory for the Study of Arctic Climate Expedition. Arctic Data Center. DOI: http://dx.doi.org/10.18739/A2XK84R5C; https://arcticdata.io/catalog/view/doi:10.18739/A2XK84R5C.
- **Crocker, GB.** 1984. The physical properties of snowcover on sea ice in the Central High Arctic [Master's thesis]. Montreal, Canada: McGill University.
- Danabasoglu, G. Lamarque, JF, Bacmeister, J. Bailey, DA, DuVivier, AK, Edwards, J, Emmons, LK, Fasullo, J., Garcia, R., Gettelman, A., Hannay, C., Holland, MM, Large, WG, Lauritzen, PH, Lawrence, DM, Lenaerts, JTM, Lindsay, K, Lipscomb, WH, Mills, MJ, Neale, R, Oleson, KW, Otto-Bliesner, B, Phillips, AS, Sacks, W, Tilmes, S, van Kampenhout, L. Vertenstein, M. Bertini, A. Dennis, J. Deser, C. Fischer, C. Fox-Kemper, B. Kay, JE, Kinnison, D, Kushner, PJ, Larson, VE, Long, MC, Mickelson, S, Moore, JK, Nienhouse, E, Polvani, L, Rasch, PJ, Strand, WG. 2020. The Community Earth System Model Version 2 (CESM2). *Journal of Advances in Modeling Earth Systems* **12**(2): e2019MS001916. DOI: http://dx.doi.org/10.1029/ 2019MS001916; https://onlinelibrary.wiley.com/ doi/abs/10.1029/2019MS001916.
- **Déry, SJ, Tremblay, LB.** 2004. Modeling the effects of wind redistribution on the snow mass budget of polar sea ice. *Journal of Physical Oceanography* **34**(1): 258–271. DOI: http://dx.doi.org/10.1175/1520-0485(2004)034<0258:MTEOWR>2.0.CO;2; https://journals.ametsoc.org/view/journals/phoc/34/1/1520-0485_2004_034_0258_mteowr_2.0. co 2.xml.
- **Déry, SJ, Yau, MK**. 1999. A climatology of adverse winter-type weather events. *Journal of Geophysical*

- *Research: Atmospheres* **104**(D14): 16657–16672. DOI: http://dx.doi.org/10.1029/1999JD900158; https://onlinelibrary.wiley.com/doi/abs/10.1029/1999JD900158.
- DuVivier, AK, Holland, MM, Kay, JE, Tilmes, S, Gettelman, A, Bailey, DA. 2020. Arctic and Antarctic Sea ice mean state in the Community Earth System Model Version 2 and the influence of atmospheric chemistry. *Journal of Geophysical Research: Oceans* 125(8): e2019JC015934. DOI: http://dx.doi.org/10.1029/2019JC015934; https://onlinelibrary.wiley.com/doi/abs/10.1029/2019JC015934.
- Eyring, V, Bony, S, Meehl, GA, Senior, CA, Stevens, B, Stouffer, RJ, Taylor, KE. 2016. Overview of the Coupled Model Intercomparison Project Phase 6 (CMIP6) experimental design and organization. *Geoscientific Model Development* **9**(5): 1937–1958. DOI: http://dx.doi.org/10.5194/gmd-9-1937-2016; https://gmd.copernicus.org/articles/9/1937/2016/.
- Gow, AJ, Meese, DA, Perovich, DK, Tucker, WB III. 1990. The anatomy of a freezing lead. *Journal of Geophysical Research: Oceans* **95**(C10): 18221–18232. DOI: http://dx.doi.org/10.1029/JC095iC10p18221; https://onlinelibrary.wiley.com/doi/abs/10.1029/JC095iC10p18221.
- **Hanson, AM**. 1980. The snow cover of sea ice during the arctic ice dynamics joint experiment, 1975 to 1976. *Arctic and Alpine Research* **12**(2): 215–226. DOI: http://dx.doi.org/10.1080/00040851.1980.1200 4180; https://www.tandfonline.com/doi/abs/10. 1080/00040851.1980.12004180.
- Holland, MM, Clemens-Sewall, D, Landrum, L, Light, B, Perovich, D, Polashenski, C, Smith, M, Webster, M. 2021. The influence of snow on sea ice as assessed from simulations of CESM2. *The Cryosphere* **15**(10): 4981–4998. DOI: http://dx.doi.org/10. 5194/tc-15-4981-2021; https://tc.copernicus.org/articles/15/4981/2021/.
- **Hunke, EC**, **Hebert, DA**, **Lecomte, O**. 2013. Level-ice melt ponds in the Los Alamos sea ice model, CICE. *Ocean Modelling* **71**: 26–42. DOI: http://dx.doi. org/10.1016/j.ocemod.2012.11.008; https://www.sciencedirect.com/science/article/pii/S1463 500312001680.
- Hunke, EC, Lipscomb, W, Jones, P, Turner, A, Jeffery, N, Elliott, S. 2017. CICE, the Los Alamos sea ice model. Los Alamos, NM: Los Alamos National Laboratory. Available at https://www.osti.gov/biblio/1364126.
- Kay, JE, DeRepentigny, P, Holland, MM, Bailey, DA, DuVivier, AK, Blanchard-Wrigglesworth, E, Deser, C, Jahn, A, Singh, H, Smith, MM, Webster, MA, Edwards, J, Lee, SS, Rodgers, KB, Rosenbloom, N. 2022. Less surface sea ice melt in the CESM2 improves Arctic sea ice simulation with minimal non-polar climate impacts. *Journal of Advances in Modeling Earth Systems* 14(4): e2021MS002679. DOI: http://dx.doi.org/10.1029/2021MS002679; https://onlinelibrary.wiley.com/doi/abs/10.1029/2021MS002679.

- Keen, A, Blockley, E, Bailey, DA, Boldingh Debernard, J, Bushuk, M, Delhaye, S, Docquier, D, Feltham, D, Massonnet, F, O'Farrell, S, Ponsoni, L, Rodriguez, JM, Schroeder, D, Swart, N, Toyoda, T, Tsujino, H, Vancoppenolle, M, Wyser, K. 2021. An intercomparison of the mass budget of the Arctic sea ice in CMIP6 models. *The Cryosphere* 15(2): 951–982. DOI: http://dx.doi.org/10.5194/tc-15-951-2021; https://tc.copernicus.org/articles/15/951/2021/.
- Lecomte, O, Fichefet, T, Flocco, D, Schroeder, D, Vancoppenolle, M. 2015. Interactions between wind-blown snow redistribution and melt ponds in a coupled ocean—sea ice model. *Ocean Modelling* **87**: 67–80. DOI: http://dx.doi.org/10.1016/j. ocemod.2014.12.003; https://www.sciencedirect.com/science/article/pii/S1463500314001784.
- Lecomte, O, Fichefet, T, Vancoppenolle, M, Domine, F, Massonnet, F, Mathiot, P, Morin, S, Barriat, PY. 2013. On the formulation of snow thermal conductivity in large-scale sea ice models. *Journal of Advances in Modeling Earth Systems* **5**(3): 542–557. DOI: http://dx.doi.org/10.1002/jame.20039; https://agupubs.onlinelibrary.wiley.com/doi/abs/10.1002/jame.20039.
- **Ledley, TS**. 1991. Snow on sea ice: Competing effects in shaping climate. *Journal of Geophysical Research: Atmospheres* **96**(D9): 17195–17208. DOI: http://dx.doi.org/10.1029/91JD01439; https://agupubs.onlinelibrary.wiley.com/doi/abs/10.1029/91JD0 1439.
- **Leonard, KC**, **Maksym, T**. 2011. The importance of windblown snow redistribution to snow accumulation on Bellingshausen Sea ice. *Annals of Glaciology* **52**(57): 271–278. DOI: http://dx.doi.org/10.3189/1727564 11795931651. Available at https://www.cambridge. org/core/journals/annals-of-glaciology/article/ importance-of-windblown-snow-redistribution-tosnow-accumulation-on-bellingshausen-sea-ice/ 4BDFC34361C599B250C071188A52FF0C.
- **Lipscomb, WH.** 2001. Remapping the thickness distribution in sea ice models. *Journal of Geophysical Research: Oceans* **106**(C7): 13989–14000. DOI: http://dx.doi.org/10.1029/2000JC000518; https://onlinelibrary.wiley.com/doi/abs/10.1029/2000JC000518.
- **Loschilov, V.** 1964. Snow cover on the ice of the central Arctic. *Problemy Arktiki i Antarktiki* **17**: 36–45.
- Maykut, GA. 1982. Large-scale heat exchange and ice production in the central Arctic. *Journal of Geophysical Research: Oceans* 87(C10): 7971–7984. DOI: http://dx.doi.org/10.1029/JC087iC10p07971; https://agupubs.onlinelibrary.wiley.com/doi/abs/10.1029/JC087iC10p07971.
- Maykut, GA, Untersteiner, N. 1971. Some results from a time-dependent thermodynamic model of sea ice. *Journal of Geophysical Research* **76**(6): 1550–1575. DOI: http://dx.doi.org/10.1029/JC076i006p01550; https://agupubs.onlinelibrary.wiley.com/doi/abs/10.1029/JC076i006p01550.

- Nicolaus, M, Perovich, DK, Spreen, G, Granskog, MA, von Albedyll, L, Angelopoulos, M, Anhaus, P, Arndt, S, Belter, HJ, Bessonov, V, Birnbaum, G, Brauchle, J, Calmer, R, Cardellach, E, Cheng, B, Clemens-Sewall, D. Dadic, R. Damm, E. de Boer, G. Demir, O. Dethloff, K. Divine, DV, Fong, AA, Fons, S, Frey, MM, Fuchs, N, Gabarró, C, Gerland, S, Goessling, HF, Gradinger, R, Haapala, J, Haas, C, Hamilton, J, Hannula, HR, Hendricks, S, Herber, A. Heuzé, C. Hoppmann, M. Høyland, KV, Huntemann, M. Hutchings, JK, Hwang, B. Itkin, P, Jacobi, HW, Jaggi, M, Jutila, A, Kaleschke, L, Katlein, C, Kolabutin, N, Krampe, D, Kristensen, SS, Krumpen, T, Kurtz, N, Lampert, A, Lange, BA, Lei, R, Light, B, Linhardt, F, Liston, GE, Loose, B, Macfarlane, AR, Mahmud, M, Matero, IO, Maus, S, Morgenstern, A, Naderpour, R, Nandan, V, Niubom, A. Oggier, M. Oppelt, N. Pätzold, F. Perron, C, Petrovsky, T, Pirazzini, R, Polashenski, C, Rabe, B, Raphael, IA, Regnery, J, Rex, M, Ricker, R, Riemann-Campe, K, Rinke, A, Rohde, J, Salganik, E, Scharien, RK, Schiller, M, Schneebeli, M, Semmling, M, Shimanchuk, E, Shupe, MD, Smith, MM, Smolyanitsky, V, Sokolov, V, Stanton, T, Stroeve, J, Thielke, L, Timofeeva, A, Tonboe, RT, Tavri, A, Tsamados, M. Wagner, DN, Watkins, D. Webster, M, Wendisch, M. 2022. Overview of the MOSAiC expedition: Snow and sea ice. Elementa: Science of *the Anthropocene* **10**(1): 000046. DOI: http://dx.doi. org/10.1525/elementa.2021.000046.
- Nixdorf, U, Dethloff, K, Rex, M, Shupe, M, Sommerfeld, A, Perovich, DK, Nicolaus, M, Heuzé, C, Rabe, B, Loose, B, Damm, E, Gradinger, R, Fong, A, Maslowski, W, Rinke, A, Kwok, R, Spreen, G, Wendisch, M, Herber, A, Hirsekorn, M, Mohaupt, V, Frickenhaus, S, Immerz, A, Weiss-Tuider, K, König, B, Mengedoht, D, Regnery, J, Gerchow, P, Ransby, D, Krumpen, T, Morgenstern, A, Haas, C, Kanzow, T, Rack, FR, Saitzev, V, Sokolov, V, Makarov, A, Schwarze, S, Wunderlich, T, Wurr, K, Boetius, A. 2021. MOSAiC extended acknowledgement. DOI: http://dx.doi.org/10.5281/zenodo. 5541624; https://zenodo.org/record/5541624.
- **Perovich, DK**. 1991. Seasonal changes in sea ice optical properties during fall freeze-up. *Cold Regions Science and Technology* **19**(3): 261–273. DOI: http://dx.doi.org/10.1016/0165-232X(91)90041-E; https://www.sciencedirect.com/science/article/pii/0165232X9 190041E.
- **Perovich, DK, Richter-Menge, JA**. 1994. Surface characteristics of lead ice. *Journal of Geophysical Research: Oceans* **99**(C8): 16341–16350. DOI: http://dx.doi.org/10.1029/94JC01194; https://agupubs.online library.wiley.com/doi/abs/10.1029/94JC01194.
- Petty, AA, Holland, MM, Bailey, DA, Kurtz, NT. 2018. Warm Arctic, increased winter sea ice growth? *Geophysical Research Letters* **45**(23): 12922–12930. DOI: http://dx.doi.org/10.1029/2018GL079223; https://onlinelibrary.wiley.com/doi/abs/10.1029/2018GL079223.

- Radionov, VF, Bryazgin, NN, Alexandrov, EI. 1997. The snow cover of the Arctic basin [Technical Report APL-UW TR9701]. Seattle, WA: Applied Physics Laboratory, University of Washington. Available at https://apps.dtic.mil/sti/citations/ADA327057.
- Raphael, I, Clemens-Sewall, D, Perovich, D, Polashenski, C, Itkin, P, Regnery, J, Nicolaus, M, Jaggi, M, Smith, M, Matero, I, Macfarlane, A, Hutchings, J, Jutila, A, Fons, S, Oggier, M, Wagner, D, Demir, O. 2022. Measurements of sea ice point-mass-balance using hotwire thickness gauges and ablation stakes during the Multidisciplinary Drifting Observatory for the Study of Arctic Climate (MOSAiC) Expedition in the Central Arctic (2019–2020). Arctic Data Center. DOI: http://dx.doi.org/10.18739/A2NK36626; https://arcticdata.io/catalog/view/doi%3A10.18739%2FA2NK36626.
- Ricker, R, Kauker, F, Schweiger, A, Hendricks, S, Zhang, J, Paul, S. 2021. Evidence for an increasing role of ocean heat in Arctic winter sea ice growth. *Journal of Climate* **34**(13): 5215–5227. DOI: http://dx.doi.org/10.1175/JCLI-D-20-0848.1; https://journals.ametsoc.org/view/journals/clim/34/13/JCLI-D-20-0848.1.xml.
- Rösel, A, Itkin, P, King, J, Divine, D, Wang, C, Granskog, MA, Krumpen, T, Gerland, S. 2018. Thin sea ice, thick snow, and widespread negative freeboard observed during N-ICE2015 north of Svalbard. *Journal of Geophysical Research: Oceans* 123(2): 1156–1176. DOI: http://dx.doi.org/10.1002/2017J C012865; https://onlinelibrary.wiley.com/doi/abs/10.1002/2017JC012865.
- Schröder, D, Feltham, DL, Tsamados, M, Ridout, A, Tilling, R. 2019. New insight from CryoSat-2 sea ice thickness for sea ice modelling. *The Cryosphere* **13**(1): 125–139. DOI: http://dx.doi.org/10.5194/tc-13-125-2019; https://tc.copernicus.org/articles/13/125/2019/.
- **Semtner, AJ**. 1976. A model for the thermodynamic growth of sea ice in numerical investigations of climate. *Journal of Physical Oceanography* **6**(3): 379–389. DOI: http://dx.doi.org/10.1175/1520-0485(1976)006<0379:AMFTTG>2.0.CO;2; https://journals.ametsoc.org/view/journals/phoc/6/3/1520-0485_1976_006_0379_amfttg_2_0_co_2.xml.
- Smith, M, Light, B, Perovich, D, Webster, M, Anhaus, P, Clemens-Sewall, D, Linhardt, F, Macfarlane, A, Raphael, I, Bozzato, D, Brasseur, Z, Dadic, R, Fons, S, Immerz, A, Hannula, HR, Hutchings, J, Pätzold, F, Regnery, J, Pirazzini, R, Tavri, A. 2021. Raw files for broadband and spectral albedo measurements of the sea ice surface during the Multidisciplinary drifting Observatory for the Study of Arctic Climate (MOSAiC) campaign in the Central Arctic Ocean, April–September 2020. Arctic Data Center. DOI: http://dx.doi.org/10.18739/A2ZG 6G81T; https://arcticdata.io/catalog/view/doi%3A 10.18739%2FA2ZG6G81T.
- **Spreen, G, Kwok, R, Menemenlis, D, Nguyen, AT**. 2017. Sea-ice deformation in a coupled ocean–sea-ice

- model and in satellite remote sensing data. *The Cryosphere* **11**(4): 1553–1573. DOI: http://dx.doi.org/10.5194/tc-11-1553-2017; https://tc.copernicus.org/articles/11/1553/2017/.
- Sturm, M, Holmgren, J, Perovich, DK. 2002a. Winter snow cover on the sea ice of the Arctic Ocean at the Surface Heat Budget of the Arctic Ocean (SHEBA): Temporal evolution and spatial variability. *Journal of Geophysical Research: Oceans* 107(C10): SHE 23–1–SHE 23–17. DOI: http://dx.doi.org/10. 1029/2000JC000400; https://agupubs.online library.wiley.com/doi/abs/10.1029/2000JC00 0400.
- Sturm, M, Perovich, DK, Holmgren, J. 2002b. Thermal conductivity and heat transfer through the snow on the ice of the Beaufort Sea. *Journal of Geophysical Research: Oceans* **107**(C10): SHE 19–1–SHE 19–17. DOI: http://dx.doi.org/10.1029/2000JC000409; https://agupubs.onlinelibrary.wiley.com/doi/abs/10.1029/2000JC000409.
- Thielke, L, Huntemann, M, Hendricks, S, Jutila, A, Ricker, R, Spreen, G. 2021. Helicopter-borne thermal infrared sea ice surface temperature images during the MOSAiC expedition, NetCDF format. *PANGAEA*. DOI: http://dx.doi.org/10.1594/PANGAEA.934658.

- Thorndike, AS, Rothrock, DA, Maykut, GA, Colony, R. 1975. The thickness distribution of sea ice. *Journal of Geophysical Research* (1896–1977) **80**(33): 4501–4513. DOI: http://dx.doi.org/10.1029/JC0 80i033p04501; https://onlinelibrary.wiley.com/doi/abs/10.1029/JC080i033p04501.
- **Turner, AK, Hunke, EC**. 2015. Impacts of a mushy-layer thermodynamic approach in global sea-ice simulations using the CICE sea-ice model. *Journal of Geophysical Research: Oceans* **120**(2): 1253–1275. DOI: http://dx.doi.org/10.1002/2014JC010358; https://onlinelibrary.wiley.com/doi/abs/10.1002/2014JC010358.
- Urrego-Blanco, JR, Urban, NM, Hunke, EC, Turner, AK, Jeffery, N. 2016. Uncertainty quantification and global sensitivity analysis of the Los Alamos Sea Ice Model. *Journal of Geophysical Research: Oceans* 121(4): 2709–2732. DOI: http://dx.doi.org/10.1002/2015JC011558; https://agupubs.onlinelibrary.wiley.com/doi/abs/10.1002/2015JC011558.
- Webster, M, Gerland, S, Holland, M, Hunke, E, Kwok, R, Lecomte, O, Massom, R, Perovich, D, Sturm, M. 2018. Snow in the changing sea-ice systems. *Nature Climate Change* **8**(11): 946–953. DOI: http://dx.doi.org/10.1038/s41558-018-0286-7; https://www.nature.com/articles/s41558.

How to cite this article: Clemens-Sewall, D, Smith, MM, Holland, MM, Polashenski, C, Perovich, D. 2022. Snow redistribution onto young sea ice: Observations and implications for climate models. *Elementa: Science of the Anthropocene* 10(1). DOI: https://doi.org/10.1525/elementa.2021.00115

Domain Editor-in-Chief: Jody W. Deming, University of Washington, Seattle, WA, USA

Guest Editor: Marcel Nicolaus, Alfred-Wegener-Institut Helmholtz-Zentrum für Polar- und Meeresforschung, Bremerhaven, Germany

Knowledge Domain: Ocean Science

Part of an Elementa Special Feature: The Multidisciplinary Drifting Observatory for the Study of Arctic Climate (MOSAiC)

Published: September 8, 2022 Accepted: August 3, 2022 Submitted: December 7, 2021

Copyright: © 2022 The Author(s). This is an open-access article distributed under the terms of the Creative Commons Attribution 4.0 International License (CC-BY 4.0), which permits unrestricted use, distribution, and reproduction in any medium, provided the original author and source are credited. See http://creativecommons.org/licenses/by/4.0/.

